On a 3D material modelling of smart nanocomposite structures

Mohammad Malikan [a,*], Shahriar Dastjerdi [b,c], Victor A. Eremeyev [a,d], Hamid M. Sedighi [e,f]

[a] *Department of Mechanics of Materials and Structures, Faculty of Civil and Environmental Engineering, Gdańsk University of Technology, ul. Gabriela Narutowicza 11/12, Gdańsk 80-233, Poland*
[b] *Akdeniz University, Civil Engineering Department, Division of Mechanics, Antalya, Turkey*
[c] *Department of Mechanical Engineering, Ferdowsi University of Mashhad, Mashhad 91775-1111, Iran*
[d] *Department of Civil and Environmental Engineering and Architecture(DICAAR), University of Cagliari, Via Marengo, 2, Cagliari 09123, Italy*
[e] *Mechanical Engineering Department, Faculty of Engineering, Shahid Chamran University of Ahvaz, Ahvaz, Iran*
[f] *Drilling Center of Excellence and Research Center, Shahid Chamran University of Ahvaz, Ahvaz, Iran*

ARTICLE INFO

ABSTRACT

Smart composites (SCs) are utilized in electro-mechanical systems such as actuators and energy harvesters. Typically, thin-walled components such as beams, plates, and shells are employed as structural elements to achieve the mechanical behavior desired in these composites. SCs exhibit various advanced properties, ranging from lower order phenomena like piezoelectricity and piezomagneticity, to higher order effects including flexoelectricity and flexomagneticity. The recently discovered flexomagneticity in smart composites has been investigated under limited conditions. A review of the existing literature indicates a lack of evaluation in three-dimensional (3D) elasticity analysis of SCs when the flexomagnetic effect (FM) exists. To address this issue, the governing equations will incorporate the term $\partial/\partial z$, where z represents the thickness coordinate. The variational technique will guide us in further developing these governing equations. By using hypotheses and theories such as a 3D beam model, von Kármán's strain nonlinearity, Hamilton's principle, and well-established direct and converse FM models, we will derive the constitutive equations for a thick composite beam. Conducting a 3D analysis implies that the strain and strain gradient tensors must be expressed in 3D forms. The inclusion of the term $\partial/\partial z$ necessitates the construction of a different model. It should be noted that current commercial finite element codes are not equipped to accurately and adequately handle micro- and nano-sized solids, thus making it impractical to model a flexomagnetic composite structure using these programs. Therefore, we will transform the derived characteristic linear three-dimensional bending equations into a 3D semi-analytical Polynomial domain to obtain numerical results. This study demonstrates the importance of conducting 3D mechanical analyses to explore the coupling effects of multiple physical phenomena in smart structures.

1. Introduction

A reciprocity of the modern smart composite structures with the non-smart advanced ones (functionally graded structures, nanocomposites, etc.) marks that the smart composites are capable of remembering the configurations, and then under specific stimuli

---

* Corresponding author.
E-mail address: mohammad.malikan@pg.edu.pl (M. Malikan).

Nomenclature

N_0	Axial effect of magnetic field
u	Axial displacement
ε_{xx}	Axial strain
σ_{xx}	Axial stress
$\aleph$	Displacements
$u_i (i=1,3)$	Displacement in the x- and z- directions
ε_{ij}	Elastic strains
σ_{ij}	Elastic stresses
ψ	External magnetic potential
F	External mass loads
h_{ijkl}	4th-order converse flexomagnetic tensor
f_{ijkl}	4th-order direct flexomagnetic tensor
C_{ijkl}	4th-order elasticity tensor
$\Re$	Free energy density
η_{ijk}	Gradient of the elastic strains
ξ_{ijk}	Higher-order stress tensor
T_{ij}	Hyper stress resultant
δ_{ij}	Kronecker's delta
w	Lateral displacement
q	Lateral static load
x	Length coordinate
L	Length of the beam
H_i	Magnetic field
B_i	Magnetic flux
l	Material's length scale parameter
Ψ	Magnetic potential function
ν	Poisson's ratio
α	Position vector
G	Shear modulus
τ_{xz}	Shear stress
γ_{xz}	Shear strain
U	Strain energy
t	Surface traction
a_{ij}	2nd-order magnetic permeability tensor
g_{ijklmn}	6th-order strain gradient tensor
g_i	Strain gradient coefficients
q_{ijk}	3rd-order piezomagnetic tensor
z	Thickness coordinate
h	Thickness of the beam
ε_{zz}	Transverse strain
σ_{zz}	Transverse stress
∇	3D nabla operator
p	Unknown variables for displacements
N_{xx}	Work done by a magnetic field
W	Work performed by external forces
b	Width of the beam
E	Young's modulus

can return to their initial situations [Mohamed, 2017]. In other words, it can be said that smart materials and structures are objects that sense circumstance conditions and react to the environment by processing the obtained information. Having such a sense of the surroundings enables smart materials to be suitably responsive and reactive. The other side, non-smart advanced composites are usually multi-structural solid elements whose utilizations provide multi-functionality [Xu et al., 2021a, X., 2021b; Shao Ong et al., 2023; Yee & Ghayesh, 2023; Karami & Ghayesh, 2023]. Although such structures remit extraordinary mechanical features, they are senseless to the non-solid operators. For instance, electric and magnetic fields, or humidity and temperature parameters.

Today, electro-magnetic materials are broadly used in various industries and have found important applications in many engineering branches and disciplines, such as sensors and actuators. Intelligent structures have expanded technologies to produce non-

biological systems in such a way that their integrated design can be achieved by using extensive observations in biological systems and competition with adaptive capabilities. Among the smart materials widely used in structures, one can mention smart composite (SC) beam-like structures. Smart composite beams are advanced structural elements that combine the benefits of both composite materials and smart systems. They are made by integrating different materials, such as ceramics, boron, cobalt, micro/nanostructures, etc., to be embedded as sensors, actuators, and control systems. The application of these materials can be seen in an outspread range to eliminate vibration, noise, and shape control in civil, mechanical, marine, and aerospace structures [Vijay et al., 2006; Poplawski et al., 2021; Ezzin et al., 2022; Markov et al., 2022; Gia et al., 2022]. These smart elements enable the beam to adapt to changing loads and environmental conditions, as well as to actively respond to external stimuli such as vibrations or impacts. Smart composite beams have other large assortments of applications, including in aerospace, civil infrastructure, and automotive industries, particularly in renewable energy. They offer improved durability, damage tolerance, and corrosion resistance compared to classic materials, and their smartness makes them ideal for structures that must adapt to changing conditions or respond to dynamic loads [Fattahi & Mirdamadi, 2017; Singhal et al., 2021; Singh et al., 2022; Ud Din et al., 2022; Jankowski, 2022].

A property that causes smartness in the composite beams can be the flexomagnetic effect. Flexomagneticity is a relatively new area of research in the mechanics of solids. It constitutes a fundamental property by which a material exhibits a magnetic response to the gradient of mechanical strain (direct effect) or emerges due to the coupling between the gradient of magnetic field and mechanical strain (reverse effect). This scale-dependent coupling has been observed in a broad spectrum of materials, consisting of ceramics, insulators, and even biological systems. The phenomenon has the potential to revolutionize several fields, encompassing magneto-elasticity, spintronics, and magnetic data storage. Further research in this field could lead to the development of new materials with enhanced magnetic properties that can be controlled and manipulated using mechanical deformation [Lukashev & Sabirianov, 2010; Sabirianov & Lukashev, 2010; Kabychenkov & Lisovskii, 2019; Eliseev et al., 2009, 2011, 2019]. One example of the use of the flexomagnetic effect is in the development of magnetoelectric sensors. These sensors use the flexomagnetic effect to convert the gradient of mechanical strain into an electrical signal, allowing them to detect changes in pressure, temperature, or other environmental factors. Another application is in the development of materials that can convert mechanical energy into the electrical one. By using the flexomagnetic effect, it may be possible to develop materials that can harvest energy from mechanical vibrations, such as those generated by the movement of machinery or the motion of a human body [Hong Lee et al., 2017; Makushko et al., 2022; Borkar et al., 2022; Mallek-Zouari et al., 2023].

The theoretical understanding of the flexomagnetic effect is still in its early stages, with much of the work being done using computational models. However, experimental studies have provided strong evidence for the existence of the effect and have demonstrated its potential for practical applications [Lukashev & Sabirianov, 2010; Sabirianov & Lukashev, 2010; Hong Lee et al., 2017; Kabychenkov & Lisovskii, 2019; Eliseev et al., 2009, 2011, 2019; Makushko et al., 2022; Borkar et al., 2022; Mallek-Zouari et al., 2023]. As research in the field continues, it is likely that new materials and devices will be developed that make use of the flexomagnetic effect, leading to new opportunities for the development of novel technologies. Research has focused on developing flexomagneticity in several conditions for materials underhand as well as understanding the fundamental mechanisms that govern their behavior in one-dimensional (1D) or two-dimensional (2D) elasticity analyses [Sidhardh & Ray, 2018; Zhang et al., 2022a, 2019, 2022; Sladek et al., 2021; Malikan & Eremeyev, 2020a, M. 2020b, 2020c; Malikan et al., 2020a, M. 2020b; Malikan & Eremeyev, 2021a, M. 2021b, M. 2021c, 2021d; Malikan et al., 2021, 2022a, M. 2022b; Malikan & Eremeyev, 2022a, M. 2022b; Malikan & Eremeyev, 2023a; Khabisi-Momeni & Tahani, 2022]. These literature backgrounds provide a good starting point for learning about the field of flexomagnetic and its current state of research. Some of the challenges that still remain, include improving the efficiency of energy conversion, developing new fabrication techniques, and upgrading the durability and stability of these materials. Overall, flexomagnetic is a promising field of research with many potential applications. However, more studies are essential to fully realize the potential of FM materials and develop practical devices that can take advantage of their unique properties.

Three-dimensional (3D) elasticity analysis is a mathematical and computational approach used to model the behavior of solid objects in three dimensions. Three-dimensional elasticity analysis offers several advantages over simpler two-dimensional models [Wittrick, 1987; Liew & Yang, 1999; Dastjerdi & Akgöz, 2018; Russillo et al., 2022] which are composed of:

1. More accurate results: Three-dimensional models (3DMs) take into account the full geometry of the object being analyzed, allowing for more precise results. In contrast, two-dimensional models may not capture the full complexity of the object and can lead to erroneous or incomplete results.
2. Greater flexibility: 3DMs offer greater flexibility in terms of the types of boundary conditions and loads that can be applied. This can be critical for analyzing a wide range of different scenarios and applications.
3. Better representation of real-world conditions: 3DMs are better able to capture the full range of deformation and motion that occurs in real-world structures and objects. This is consequential for minutely predicting how a structure will behave under different conditions.

A three-dimensional elasticity analysis of flexomagnetic smart structures is covered in this report. The modified energy density of piezo-flexomagnetic (PFM) beams newly derived by the author of this paper will be reused. Thereafter, the constitutive equations will appear step by step. All the 3D tensors will be collected and seized through the existing and well-esteemed literature. Due to the 3D formulation of elastic non-constant thickness beams, the internal forces and moments cannot be developed. Instead of these, the principal equations can be attained directly via stress components. The transverse static load is presumed to act uniformly. The possible solution for the 3D equilibrium equations can be accomplished through polynomial series based on a semi-analytical process.

The paper's layout is organized as follows:

Section 1 is dedicated to an introduction to the topic together with a short literature review.
Section 2 represents the mathematical modeling of the objective title.
Section 3 denotes a solution technique process that is based on a semi-analytical method.
Section 4 compares the results in conformity with the references.
Section 5 discusses the results and puts out a detailed interpretation.
Section 6 provides conclusions and a summary of the performed study.

2. Mathematical modelling

Fig. 1 shows a composite beam, positioned in the *x-z* coordinate system and occupying a block volume of $[0, L] \times [-0.5h, 0.5h]$. The beam is subjected to a transverse static load and a magnetic field that exhibits a linear variation across its thickness. It is noted that the length "*L*" inside the formulations is the effective length of the beam.

2.1. The flexomagnetic model

Let us briefly examine the mathematical models available for FM structures [M. Malikan & Eremeyev, 2022b]. These samples are limited to small deformations and an initial isothermal condition. The vectors of displacement ($\aleph$) variables and first-order magnetic field (*H*) are given by

$$\aleph = \aleph(\alpha), \mathrm{H} = \mathrm{H}(\alpha) \tag{1}$$

where the α is a position vector.

The general quadratic representation of the free energy density of the flexomagnetic structures is given by [M. Malikan & Eremeyev, 2022b]

$$\Re = \frac{1}{2}C_{ijkl}\varepsilon_{ij}\varepsilon_{kl} - \frac{1}{2}a_{kl}H_kH_l - q_{ijk}\varepsilon_{ij}H_k + \frac{1}{2}g_{ijklmn}\frac{\partial\varepsilon_{ij}}{\partial x_k}\frac{\partial\varepsilon_{lm}}{\partial x_n} + r_{ijklm}\varepsilon_{ij}\frac{\partial\varepsilon_{kl}}{\partial x_m}$$
$$- \frac{1}{2}b_{ijkl}\frac{\partial H_i}{\partial x_j}\frac{\partial H_k}{\partial x_l} - s_{ijk}H_i\frac{\partial H_j}{\partial x_k} - \lambda_{ijklm}\frac{\partial\varepsilon_{ij}}{\partial x_k}\frac{\partial H_l}{\partial x_m} - \frac{1}{2}f_{ijkl}\frac{\partial\varepsilon_{ij}}{\partial x_k}H_l - \frac{1}{2}h_{ijkl}\varepsilon_{ij}\frac{\partial H_k}{\partial x_l} \tag{2}$$

in which the utilized tensors can be introduced as follows:

C_{ijkl}: 4th order pure elasticity tensor
a_{kl}: 2nd order magnetic permeability tensor
q_{ijk}: 3rd order piezomagnetic tensor
b_{ijkl}: 4th order magnetic field gradients coupling tensor
g_{ijklmn}: 6th order strain gradient tensor
λ_{ijklm}: 5th order strain gradient-magnetic field gradient coupling tensor
s_{ijk}: 3rd order magnetic field-magnetic field gradient coupling tensor
r_{ijklm}: 5th order strain-strain gradient coupling tensor
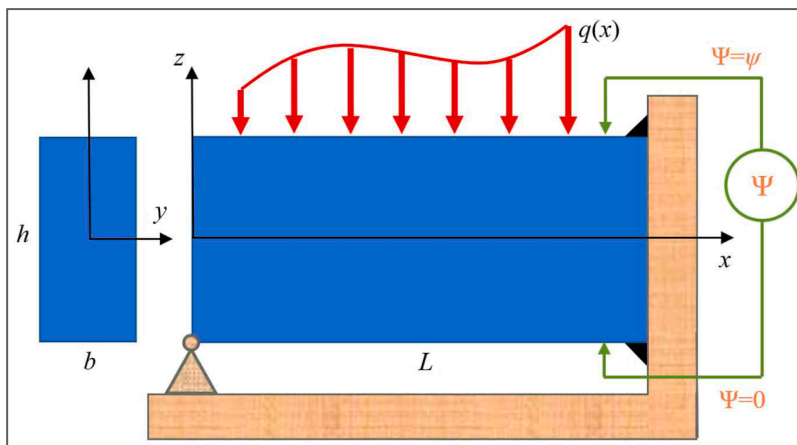h_{ijkl}: 4th order converse flexomagnetic tensor

Fig. 1. A symbolic thick continuum multi-physic simply supported-clamped beam.

f_{ijkl}: 4th order direct flexomagnetic tensor

The first three terms in Eq. (2) correspond to piezomagnetic materials. Not to mention that the first term also expresses a pure elastic structure. Some of the above-written tensors are supposed to be ignored for centrosymmetric materials, such as q_{ijk} and λ_{ijklm}. In particular, for centrosymmetric materials, the piezomagnetic effect does not exist. Nevertheless, these materials include f_{ijkl} and h_{ijkl}. The structure investigated in this work is referred to as a non-centrosymmetric piezomagnetic solid.

The variables presented in Eq. (2) are given by the formulae

Elastic strain:

$$\varepsilon = \frac{1}{2}\left(\nabla u + \nabla u^T + \nabla u . \nabla u^T\right) \tag{3a}$$

A gradient of the elastic strain:

$$\eta = \nabla \varepsilon \tag{3b}$$

The magnetic field can be represented with the magnetic potential as

$$H = -\nabla \psi \tag{4}$$

Given the variational principle, the static characteristic equations can be associated with the problem [Malikan et al., 2020c; Xu et al., 2021c; Karami et al., 2022; Zheng et al., 2022]

$$\delta \int_V U dV = \delta W \tag{5}$$

in which V composes the domain's volume. Further, the variation of works performed by the outer forces has the following expansion:

$$\delta W = \int_V F \cdot \delta u + \int_{\partial V} t \cdot \delta u ds \tag{6}$$

The highest and lowest limits for Eq. (6) can be found by

$$\nabla .(\sigma - \nabla . \xi) + F = 0 \tag{7a}$$

$$\nabla .(B - \nabla . T) = 0 \tag{7b}$$

The piezomagnetic-flexomagnetic constitutive equations for a 3D solid involving Eq. (7) have the forms [M. Malikan & Eremeyev, 2022b]

$$\sigma_{ij} = \frac{\partial \Re}{\partial \varepsilon_{ij}} = C_{ijkl}\varepsilon_{kl} - q_{ijk}H_k + r_{ijklm}\frac{\partial \varepsilon_{kl}}{\partial x_m} - h_{ijkl}\frac{\partial H_k}{\partial x_l} \tag{8a}$$

$$\xi_{ijk} = \frac{\partial \Re}{\partial \left(\frac{\partial \varepsilon_{ij}}{\partial x_k}\right)} = g_{ijklmn}\frac{\partial \varepsilon_{lm}}{\partial x_n} + r_{ijklm}\varepsilon_{ij} - \lambda_{ijklm}\frac{\partial H_l}{\partial x_m} - f_{ijkl}H_l \tag{8b}$$

$$T_{ij} = \frac{\partial \Re}{\partial \left(\frac{\partial H_i}{\partial x_j}\right)} = -b_{ijkl}\frac{\partial H_k}{\partial x_l} - s_{ijk}H_i - \lambda_{ijklm}\frac{\partial \varepsilon_{ij}}{\partial x_k} - h_{ijkl}\varepsilon_{ij} \tag{8c}$$

$$B_i = -\frac{\partial \Re}{\partial H_i} = a_{kl}H_k + q_{ijkl}\varepsilon_{ij} + s_{ijk}\frac{\partial H_j}{\partial x_k} + f_{ijkl}\frac{\partial \varepsilon_{ij}}{\partial x_k} \tag{8d}$$

In the next part of the study, all the relations will be deduced into a beam, eliminating variables dependent on the y-axis. A thick beam is under investigation so that the representation of the 3D kinematic displacement field can be given in the below form [Malikan et al., 2018; Dastjerdi et al., 2021a; Alshenawy et al., 2023]

$$\begin{bmatrix} u_1(x,y,z) \\ u_2(x,y,z) \\ u_3(x,y,z) \end{bmatrix} = \begin{bmatrix} u(x,z) \\ 0 \\ w(x,z) \end{bmatrix} \tag{9}$$

It is easy to obtain elastic strains using the Lagrange strain formula and then the gradients of the strains [M. Malikan & Eremeyev, 2020b; Dastjerdi et al., 2020a, Sh. 2020b, Sh. 2021b]

$$\varepsilon_{ij} = \frac{1}{2}\left(\frac{\partial u_i}{\partial x_j} + \frac{\partial u_j}{\partial x_i} + \frac{\partial u_k}{\partial x_i}\frac{\partial u_k}{\partial x_j}\right); i, j, k = 1, 2, 3 \tag{10a}$$

$$\eta_{ijk} = \frac{\partial}{\partial x_k}\left[\varepsilon_{ij}\right]; i, j, k = 1, 2, 3 \tag{10b}$$

Then, the nonlinear strain and strain gradient tensors can be developed as matrices

$$[\varepsilon] = \begin{bmatrix} \varepsilon_{xx} & \varepsilon_{xy} & \varepsilon_{xz} \\ \varepsilon_{yx} & \varepsilon_{yy} & \varepsilon_{yz} \\ \varepsilon_{zx} & \varepsilon_{zy} & \varepsilon_{zz} \end{bmatrix} \tag{11a}$$

$$[\eta] = \begin{bmatrix} (\eta_{xxx} & \eta_{xxy} & \eta_{xxz}) & (\eta_{xyx} & \eta_{xyy} & \eta_{xyz}) & (\eta_{xzx} & \eta_{xzy} & \eta_{xzz}) \\ (\eta_{yxx} & \eta_{yxy} & \eta_{yxz}) & (\eta_{yyy} & \eta_{yyx} & \eta_{yyz}) & (\eta_{yzx} & \eta_{yzy} & \eta_{yzz}) \\ (\eta_{zxx} & \eta_{zxy} & \eta_{zxz}) & (\eta_{zyx} & \eta_{zyy} & \eta_{zyz}) & (\eta_{zzx} & \eta_{zzy} & \eta_{zzz}) \end{bmatrix} \tag{11b}$$

The strain and strain gradient tensors are symmetric here as $\varepsilon_{ij} = \varepsilon_{ji}$ and $\eta_{ijk} = \eta_{jik}$. Moreover, no dependence on y is considered ($\varepsilon_{xy} = \varepsilon_{yx} = \varepsilon_{yz} = \varepsilon_{zy} = 0$) as the aim is a 3D beam, not a 3D plate. Thus, we get

$$\begin{Bmatrix} \varepsilon_{xx} \\ \varepsilon_{zz} \end{Bmatrix} = \begin{Bmatrix} \frac{\partial u}{\partial x} + \frac{1}{2}\left(\frac{\partial w}{\partial x}\right)^2 \\ \frac{\partial w}{\partial z} + \frac{1}{2}\left(\frac{\partial w}{\partial z}\right)^2 \end{Bmatrix}; \{\varepsilon_{xz}\} = \{\varepsilon_{zx}\} = \frac{1}{2}\left\{\frac{\partial u}{\partial z} + \frac{\partial w}{\partial x}\left(1 + \frac{\partial w}{\partial z}\right)\right\} \tag{12}$$

And subsequently, we came to the formulae

$$\begin{Bmatrix} \eta_{xxx} \\ \eta_{xxz} \end{Bmatrix} = \begin{Bmatrix} \frac{\partial \varepsilon_{xx}}{\partial x} \\ \frac{\partial \varepsilon_{xx}}{\partial z} \end{Bmatrix} = \begin{Bmatrix} \frac{\partial^2 u}{\partial x^2} + \frac{\partial^2 w}{\partial x^2}\frac{\partial w}{\partial x} \\ \frac{\partial^2 u}{\partial x \partial z} + \frac{\partial^2 w}{\partial x \partial z}\frac{\partial w}{\partial x} \end{Bmatrix}; \begin{Bmatrix} \eta_{xzx} \\ \eta_{xzz} \end{Bmatrix} = \begin{Bmatrix} \frac{\partial \varepsilon_{xz}}{\partial x} \\ \frac{\partial \varepsilon_{xz}}{\partial z} \end{Bmatrix} = \frac{1}{2}\begin{Bmatrix} \frac{\partial^2 u}{\partial x \partial z} + \frac{\partial^2 w}{\partial x^2}\left(1 + \frac{\partial w}{\partial z}\right) + \frac{\partial w}{\partial x}\frac{\partial^2 w}{\partial x \partial z} \\ \frac{\partial^2 u}{\partial z^2} + \frac{\partial^2 w}{\partial x \partial z}\left(1 + \frac{\partial w}{\partial z}\right) + \frac{\partial w}{\partial x}\frac{\partial^2 w}{\partial z^2} \end{Bmatrix};$$

$$\begin{Bmatrix} \eta_{zxx} \\ \eta_{zxz} \end{Bmatrix} = \begin{Bmatrix} \frac{\partial \varepsilon_{zx}}{\partial x} \\ \frac{\partial \varepsilon_{zx}}{\partial z} \end{Bmatrix} = \begin{Bmatrix} \eta_{xzx} \\ \eta_{xzz} \end{Bmatrix}; \begin{Bmatrix} \eta_{zzx} \\ \eta_{zzz} \end{Bmatrix} = \begin{Bmatrix} \frac{\partial \varepsilon_{zz}}{\partial x} \\ \frac{\partial \varepsilon_{zz}}{\partial z} \end{Bmatrix} = \begin{Bmatrix} \frac{\partial^2 w}{\partial x \partial z}\left(1 + \frac{\partial w}{\partial z}\right) \\ \frac{\partial^2 w}{\partial z^2}\left(1 + \frac{\partial w}{\partial z}\right) \end{Bmatrix}; \tag{13}$$

It is now supposed to derive constitutive equations by means of Eq. (5)

$$\delta U + \delta W = 0 \tag{14}$$

For the present purposes, the strain energy variations are categorized as

$$\delta U^{All} = \delta U^{Mech} + \delta U^{Mag} \tag{15}$$

where the abbreviations of "Mech" and "Mag" denote mechanical and magnetic parts of the energy, respectively.

The variation of the mechanical part by collecting the non-zero tensors can be written as

$$\delta U^{All} = \int_V \begin{bmatrix} \sigma_{xx}\delta\varepsilon_{xx} + \tau_{xz}\delta\gamma_{xz} + \sigma_{zz}\delta\varepsilon_{zz} + \xi_{xxx}\delta\eta_{xxx} + \xi_{xxz}\delta\eta_{xxz} + \xi_{xzx}\delta\eta_{xzx} + \xi_{xzz}\delta\eta_{xzz} \\ +\xi_{zzx}\delta\eta_{zzx} + \xi_{zzz}\delta\eta_{zzz} - T_{xx}\delta\frac{\partial H_x}{\partial x} - T_{zz}\delta\frac{\partial H_z}{\partial z} - B_x\delta H_x - B_z\delta H_z \end{bmatrix} dV \tag{16}$$

where

$$H_k = \begin{Bmatrix} H_x \\ H_y \\ H_z \end{Bmatrix} = -\begin{Bmatrix} \frac{\partial\Psi}{\partial x} \\ \frac{\partial\Psi}{\partial y} \\ \frac{\partial\Psi}{\partial z} \end{Bmatrix} \tag{17}$$

Then

$$\delta U^{Mech} = \int_0^L \int_{-h/2}^{h/2} \begin{bmatrix} \sigma_{xx}\left(\dfrac{\partial \delta u}{\partial x} + \dfrac{\partial w}{\partial x}\dfrac{\partial \delta w}{\partial x}\right) + \tau_{xz}\left(\dfrac{\partial \delta u}{\partial z} + \dfrac{\partial \delta w}{\partial x} + \dfrac{\partial \delta w}{\partial x}\dfrac{\partial w}{\partial z} + \dfrac{\partial w}{\partial x}\dfrac{\partial \delta w}{\partial z}\right) \\[2mm] +\sigma_{zz}\left(\dfrac{\partial \delta u}{\partial z} + \dfrac{\partial w}{\partial z}\dfrac{\partial \delta w}{\partial z}\right) + \xi_{xxx}\left(\dfrac{\partial^2 \delta u}{\partial x^2} + \dfrac{\partial^2 \delta w}{\partial x^2}\dfrac{\partial w}{\partial x} + \dfrac{\partial^2 w}{\partial x^2}\dfrac{\partial \delta w}{\partial x}\right) \\[2mm] +\xi_{xzz}\left(\dfrac{\partial^2 \delta u}{\partial z^2} + \dfrac{\partial^2 \delta w}{\partial x\partial z} + \dfrac{\partial^2 \delta w}{\partial x\partial z}\dfrac{\partial w}{\partial z} + \dfrac{\partial^2 w}{\partial x\partial z}\dfrac{\partial \delta w}{\partial z} + \dfrac{\partial \delta w}{\partial x}\dfrac{\partial^2 w}{\partial z^2} + \dfrac{\partial w}{\partial x}\dfrac{\partial^2 \delta w}{\partial z^2}\right) \\[2mm] +\xi_{xzx}\left(\dfrac{\partial^2 \delta u}{\partial x\partial z} + \dfrac{\partial^2 \delta w}{\partial x^2} + \dfrac{\partial^2 \delta w}{\partial x^2}\dfrac{\partial w}{\partial z} + \dfrac{\partial^2 w}{\partial x^2}\dfrac{\partial \delta w}{\partial z} + \dfrac{\partial \delta w}{\partial x}\dfrac{\partial^2 w}{\partial x\partial z} + \dfrac{\partial w}{\partial x}\dfrac{\partial^2 \delta w}{\partial x\partial z}\right) \\[2mm] +\xi_{zzx}\left(\dfrac{\partial^2 \delta w}{\partial x\partial z} + \dfrac{\partial^2 \delta w}{\partial x\partial z}\dfrac{\partial w}{\partial z} + \dfrac{\partial^2 w}{\partial x\partial z}\dfrac{\partial \delta w}{\partial z}\right) \\[2mm] +\xi_{zzz}\left(\dfrac{\partial^2 \delta w}{\partial z^2} + \dfrac{\partial^2 \delta w}{\partial z^2}\dfrac{\partial w}{\partial z} + \dfrac{\partial^2 w}{\partial z^2}\dfrac{\partial \delta w}{\partial z}\right) \\[2mm] +\xi_{xxz}\left(\dfrac{\partial^2 \delta u}{\partial x\partial z} + \dfrac{\partial^2 \delta w}{\partial x\partial z}\dfrac{\partial w}{\partial x} + \dfrac{\partial^2 w}{\partial x\partial z}\dfrac{\partial \delta w}{\partial x}\right) \end{bmatrix} dzdx \tag{18a}$$

$$\delta U^{Mag} = -\int_0^L \int_{-h/2}^{h/2} \left(\frac{\partial B_x}{\partial x} + \frac{\partial B_z}{\partial z} + \frac{\partial^2 T_{xx}}{\partial x^2} + \frac{\partial^2 T_{zz}}{\partial z^2}\right)\delta\Psi dzdx + \int_{-h/2}^{h/2}\left[B_x + \frac{\partial T_{xx}}{\partial x}\right]_0^L \delta\Psi dz$$

$$+\int_0^L \left[B_z + \frac{\partial T_{zz}}{\partial z}\right]_{-h/2}^{h/2}\delta\Psi dx \tag{18b}$$

We establish the nonlinear bending equations by exerting the variational technique on Eq. (18). In consequence, we have

$$\delta u = 0; \quad \frac{\partial \sigma_{xx}}{\partial x} + \frac{\partial \tau_{xz}}{\partial z} + \frac{\partial^2 \xi_{xxx}}{\partial x^2} + \frac{\partial^2 \xi_{xxz}}{\partial x\partial z} + \frac{\partial^2 \xi_{xzx}}{\partial x\partial z} + \frac{\partial^2 \xi_{xzz}}{\partial z^2} = 0 \tag{19a}$$

$$\delta w = 0; \quad \frac{\partial \sigma_{xx}}{\partial x}\frac{\partial w}{\partial x} + \frac{\partial \sigma_{zz}}{\partial z}\left(1 + \frac{\partial w}{\partial z}\right) + \sigma_{xx}\frac{\partial^2 w}{\partial x^2} + \sigma_{zz}\frac{\partial^2 w}{\partial z^2} + \frac{\partial \tau_{xz}}{\partial x}\left(1 + \frac{\partial w}{\partial z}\right) + \frac{\partial \tau_{xz}}{\partial z}\frac{\partial w}{\partial x}$$

$$+2\tau_{xz}\frac{\partial^2 w}{\partial x\partial z} + \frac{\partial^2 \xi_{xxx}}{\partial x^2}\frac{\partial w}{\partial x} + 2\xi_{xxx}\frac{\partial^3 w}{\partial x^3} + \frac{\partial \xi_{xxx}}{\partial x}\frac{\partial^2 w}{\partial x^2} + \frac{\partial^2 \xi_{xxz}}{\partial x\partial z}\frac{\partial w}{\partial x} + 2\xi_{xxz}\frac{\partial^3 w}{\partial x^2\partial z} + \frac{\partial \xi_{xxz}}{\partial x}\frac{\partial^2 w}{\partial x\partial z}$$

$$+\frac{\partial^2 \xi_{xzx}}{\partial x^2}\left(1 + \frac{\partial w}{\partial z}\right) + 4\xi_{xzx}\frac{\partial^3 w}{\partial x^2\partial z} + \frac{\partial \xi_{xzx}}{\partial z}\frac{\partial^2 w}{\partial x^2} + \frac{\partial \xi_{xzx}}{\partial x}\frac{\partial^2 w}{\partial x\partial z} + \frac{\partial^2 \xi_{xzx}}{\partial x\partial z}\frac{\partial w}{\partial x} + \frac{\partial^2 \xi_{xzz}}{\partial x\partial z}\left(1 + \frac{\partial w}{\partial z}\right) \tag{19b}$$

$$+2\xi_{xzz}\frac{\partial^3 w}{\partial x\partial z^2} + \frac{\partial \xi_{xzz}}{\partial z}\frac{\partial^2 w}{\partial x\partial z} + \frac{\partial \xi_{xzz}}{\partial x}\frac{\partial^2 w}{\partial z^2} + 2\xi_{xzz}\frac{\partial^3 w}{\partial x\partial z^2} + \frac{\partial^2 \xi_{zzz}}{\partial z^2}\frac{\partial w}{\partial x} + \frac{\partial^2 \xi_{zzx}}{\partial x\partial z}\left(1 + \frac{\partial w}{\partial z}\right)$$

$$+2\xi_{zzx}\frac{\partial^3 w}{\partial x\partial z^2} + \frac{\partial \xi_{zzx}}{\partial z}\frac{\partial^2 w}{\partial x\partial z} + \frac{\partial^2 \xi_{zzz}}{\partial z^2}\left(1 + \frac{\partial w}{\partial z}\right) + 2\xi_{zzz}\frac{\partial^3 w}{\partial z^3} + \frac{\partial \xi_{zzz}}{\partial z}\frac{\partial^2 w}{\partial z^2} = 0$$

Based on the Voigt notation, the C_{ijkl} can be reduced into C_{ij} ($i, j \in \{1, 2, \ldots, 6\}$). The possibility of reducing the number of independent elastic constants can go forward if the material possesses a plane of elastic symmetry with a linear-elastic behavior, as [Shu et al., 2011; Qu et al., 2021; Zhang et al., 2022b; Naskar et al., 2022; Shahmohammadi et al., 2023; Zhang et al., 2023; Malikan & Eremeyev, 2023b]

$$\left[C_{ijkl}\right] = \begin{bmatrix} C_{11} & C_{12} & C_{13} & 0 & 0 & 0 \\ C_{12} & C_{22} & C_{23} & 0 & 0 & 0 \\ C_{13} & C_{23} & C_{33} & 0 & 0 & 0 \\ 0 & 0 & 0 & C_{44} & 0 & 0 \\ 0 & 0 & 0 & 0 & C_{55} & 0 \\ 0 & 0 & 0 & 0 & 0 & C_{66} \end{bmatrix} \tag{20}$$

For hexagonal crystal piezomagnetic materials, the piezomagnetic tensor can be reduced into [Malikan & Nguyen, 2018; Zhang et al., 2022b]

$$\left[q_{ijk}\right] = \begin{bmatrix} 0 & 0 & 0 & 0 & q_{15} & 0 \\ 0 & 0 & 0 & q_{15} & 0 & 0 \\ q_{31} & q_{32} & q_{33} & 0 & 0 & 0 \end{bmatrix} \tag{21}$$

in which the piezomagnetic constants were converted from q_{ijk} into $q_{i\alpha}$ ($\alpha \in \{1, 2, \ldots, 6\}$).

In the same way, the symmetry forms of the direct and reverse flexomagnetic parameters can also be reduced into three inde-

pendent elements as f_{11}, f_{111}, f_{14} for a cubic crystal [Shu et al., 2011; Qu et al., 2021; Naskar et al., 2022]

$$
[f_{ij}] = \begin{bmatrix} 0 & 0 & 0 & 0 & f_{111} & 0 \\ 0 & 0 & 0 & f_{111} & 0 & 0 \\ f_{14} & f_{14} & f_{11} & 0 & 0 & 0 \end{bmatrix}
\tag{22}
$$

Later, for the same material, as there is not enough literature, let us suppose that the converse flexomagnetic tensor corresponds to the direct one and hence it can be diminished into (the piezomagnetic material has been diagnosed to be a cubic crystal)

$$
[h_{ij}] = \begin{bmatrix} 0 & 0 & 0 & 0 & h_{46} & 0 \\ 0 & 0 & 0 & h_{46} & 0 & 0 \\ h_{15} & h_{15} & h_{11} & 0 & 0 & 0 \end{bmatrix}
\tag{23}
$$

The small-sized devices have a challenge of size dependence in their empirical design. Such small-scale characteristics can be captured using several micro- and nano-mathematical models [Dastjerdi & Jabbarzadeh, 2017; Stempin & Sumelka, 2022; Stempin et al., 2023]. In this study, the size effect is developed and exploited in the framework of the generalized first strain gradient theory. The general form of the strain gradient tensor of rank six (g_{ijklmn}) has been derived for isotropic, and linear elastic materials [Auffray et al., 2013; Zhou et al., 2016; Gusev & Lurie, 2017; Sidhardh & Ray, 2018; Torabi et al., 2021; Yurkov & Yudin, 2023]

$$
\begin{aligned}
g_{ijklmn} = & \, g_1 \left[\left(\delta_{ij}\delta_{kl} + \delta_{ik}\delta_{jl} \right)\delta_{mn} + \left(\delta_{im}\delta_{ln} + \delta_{in}\delta_{lm} \right)\delta_{jk} \right] \\
& + g_2 \left[\delta_{ij} \left(\delta_{km}\delta_{ln} + \delta_{kn}\delta_{lm} \right) + \delta_{ik} \left(\delta_{jn}\delta_{lm} + \delta_{jm}\delta_{ln} \right) \right] + g_3 \delta_{il}\delta_{jk}\delta_{mn} \\
& + g_4 \delta_{il} \left(\delta_{jm}\delta_{kn} + \delta_{jn}\delta_{km} \right) + g_5 \left[\delta_{im} \left(\delta_{jl}\delta_{kn} + \delta_{jn}\delta_{kl} \right) + \delta_{in} \left(\delta_{jl}\delta_{km} + \delta_{jm}\delta_{kl} \right) \right]
\end{aligned}
\tag{24}
$$

where g_i are the remaining higher-order elastic moduli. Remember that the solid analyzed here is a non-centrosymmetric piezo-magnetic material, but the use of the centrosymmetric strain gradient tensor is an assumption only which is implemented here for reasons of insufficient literature. The components of g are given by the isotropic gradient elasticity when the order-of-differentiation conditions and potentiality are applied.

It has been known so far that

$$
\delta_{ij} = \begin{cases} 1, & if\ i = j, \\ 0, & if\ i \neq j. \end{cases}
\tag{25}
$$

Thus, for example, we can express the first term of strain gradient elastic moduli through the Voigt notation rules as follows:

$$
g_{111111} = g_{1111} = g_{11} = 4(g_1 + g_2 + g_5) + g_3 + 2g_4
\tag{26}
$$

The material's strain gradient parameters can be expressed as follows [Zhou et al., 2016; Sidhardh & Ray, 2018; Torabi et al., 2021]:

$$
g_1 = -\frac{2}{3}(g_2 + g_5),\ g_2 = \frac{\mu}{30}\left(27l_0^2 - 4l_1^2 - 15l_2^2\right),
$$

$$
g_3 = \frac{1}{3}(8g_2 + 2g_5),\ g_4 = \frac{\mu}{3}\left(l_1^2 + 6l_2^2\right),\ g_5 = \frac{\mu}{3}\left(l_1^2 - 3l_2^2\right)
$$

in which the material length scales l_0, l_1, l_2 are introduced.

Nonetheless, we assume $l_0 = l_1 = l_2 = l$ for the sake of simplicity. In this regard, two cases can be yielded, if we adopt $l_0 = l_1 = l_2 = 0$, the attained model will exclude strain gradient effects, and by setting $l_1 = l_0 = 0$ and $l_2 = l$, the corresponding modified couple stress model will be gained. In addition, it has not yet been determined what is the exact value of the strain gradient shear modulus (μ). Hence, we consider its amount equal to the elasticity shear modulus (G) as a scalar.

Let us move ahead with the formulation. The lower and higher-order stress-strain relations can be expressed as follows:

$$
\begin{Bmatrix} \sigma_{xx} \\ \sigma_{yy} \\ \sigma_{zz} \\ \tau_{yz} \\ \tau_{xz} \\ \tau_{xy} \end{Bmatrix} = [C_{ij}]_{6\times6} \times \begin{Bmatrix} \varepsilon_{xx} \\ \varepsilon_{yy} \\ \varepsilon_{zz} \\ \gamma_{yz} \\ \gamma_{xz} \\ \gamma_{xy} \end{Bmatrix} - [q_{ij}]_{6\times3} \times \begin{Bmatrix} H_x \\ H_y \\ H_z \end{Bmatrix} - [h_{ij}]_{6\times3} \times \begin{bmatrix} \dfrac{\partial H_x}{\partial x} & 0 & 0 \\ 0 & \dfrac{\partial H_y}{\partial y} & 0 \\ 0 & 0 & \dfrac{\partial H_z}{\partial z} \end{bmatrix}
\tag{27}
$$

$$
\begin{Bmatrix} \xi_{xxx} \\ \xi_{xxz} \\ \xi_{zzx} \\ \xi_{zzz} \\ \xi_{xzz} \\ \xi_{xzx} \end{Bmatrix} = [g_{ij}]_{6\times6} \times \begin{Bmatrix} \eta_{xxx} \\ \eta_{xxz} \\ \eta_{zzx} \\ \eta_{zzz} \\ \eta_{xzz} \\ \eta_{xzx} \end{Bmatrix} - [f_{ij}]_{6\times3} \times \begin{Bmatrix} H_x \\ H_y \\ H_z \end{Bmatrix}
\tag{28}
$$

$$\begin{Bmatrix} T_{xx} \\ T_{yy} \\ T_{zz} \end{Bmatrix} = -\left[h_{ij} \right]_{3\times 6} \times \begin{Bmatrix} \varepsilon_{xx} \\ \varepsilon_{yy} \\ \varepsilon_{zz} \\ \gamma_{yz} \\ \gamma_{xz} \\ \gamma_{xy} \end{Bmatrix} \tag{29}$$

$$\begin{Bmatrix} B_x \\ B_y \\ B_z \end{Bmatrix} = \left[a_{ij} \right]_{3\times 3} \times \begin{Bmatrix} H_x \\ H_y \\ H_z \end{Bmatrix} + \left[q_{ij} \right]_{3\times 6} \times \begin{Bmatrix} \varepsilon_{xx} \\ \varepsilon_{yy} \\ \varepsilon_{zz} \\ \gamma_{yz} \\ \gamma_{xz} \\ \gamma_{xy} \end{Bmatrix} + \left[f_{ij} \right]_{3\times 6} \times \begin{Bmatrix} \eta_{xxx} \\ \eta_{xxz} \\ \eta_{zzx} \\ \eta_{zzz} \\ \eta_{xzz} \\ \eta_{xzx} \end{Bmatrix} \tag{30}$$

The expanded 3D elasticity stiffness matrix for a homogenous isotropic material can be expressed as follows [Zafarmand & Kadkhodayan, 2015; Malikan et al., 2018; Abouelregal et al., 2021; Dastjerdi et al., 2022a; Sahmani & Safaei, 2022]:

$$\left[C_{ijkl} \right] = \begin{bmatrix} \dfrac{E(1-\nu)}{K} & \dfrac{E\nu}{K} & \dfrac{E\nu}{K} & 0 & 0 & 0 \\[2mm] \dfrac{E\nu}{K} & \dfrac{E(1-\nu)}{K} & \dfrac{E\nu}{K} & 0 & 0 & 0 \\[2mm] \dfrac{E\nu}{K} & \dfrac{E\nu}{K} & \dfrac{E(1-\nu)}{K} & 0 & 0 & 0 \\[2mm] 0 & 0 & 0 & \dfrac{E}{2(1+\nu)} & 0 & 0 \\[2mm] 0 & 0 & 0 & 0 & \dfrac{E}{2(1+\nu)} & 0 \\[2mm] 0 & 0 & 0 & 0 & 0 & \dfrac{E}{2(1+\nu)} \end{bmatrix} \tag{31}$$

in which $K = (1+\nu)(1-2\nu)$.

The performed work by external loads includes the influence of the lateral magnetic field, which itself is an axial force, and the transverse static load as

$$\delta W = \int_0^L \left[q\delta w + N_{xx}\left(\frac{\partial \delta w}{\partial x}\frac{\partial w}{\partial x} \right) \right] dx \tag{32}$$

where $N_{xx} = N_0 = q_{31}\frac{\psi}{h}\displaystyle\int_{-h/2}^{h/2} d\mathbf{z}$

The determination of the values of the magnetic potential will steer the discussion. Let us define the magnetic potential on the bottom and top layers of the domain as [M. Malikan & Eremeyev, 2022b]

$$\begin{Bmatrix} \Psi\left(+\dfrac{h}{2} \right) \\[2mm] \Psi\left(-\dfrac{h}{2} \right) \end{Bmatrix} = \begin{Bmatrix} \psi \\ 0 \end{Bmatrix} \tag{33}$$

The direct FM parameter will be neglected for the next relations due to focusing on the converse FM effect only. A precise mathematical interaction between Eqs. (17), (18), (30), (33) gives (the influence of B_x has been ignored)

$$\Psi = \frac{q_{31}}{a_{33}}\left(\frac{h^2}{4} - z^2 \right)\left(\frac{\partial^2 u}{\partial x\partial z} + \frac{\partial w}{\partial x}\frac{\partial^2 w}{\partial x\partial z} \right) + \frac{q_{33}}{a_{33}}\left(\frac{h^2}{4} - z^2 \right)\left(\frac{\partial^2 w}{\partial z^2} + \frac{\partial w}{\partial z}\frac{\partial^2 w}{\partial z^2} \right) + \frac{\psi}{h}\left(z + \frac{h}{2} \right)$$

$$+ \frac{h_{46}}{a_{33}}\left(z^2 - \frac{h^2}{4} \right)\left(\frac{\partial^3 u}{\partial x^2\partial z} + \frac{\partial^3 w}{\partial x^3} + \frac{\partial^3 w}{\partial x^3}\frac{\partial w}{\partial z} + \frac{\partial w}{\partial x}\frac{\partial^3 w}{\partial x^2\partial z} \right) + \frac{h_{15}}{a_{33}}\left(z^2 - \frac{h^2}{4} \right) \tag{34}$$

$$\times \left[\frac{\partial^3 u}{\partial x\partial z^2} + \frac{\partial w}{\partial x}\frac{\partial^3 w}{\partial x\partial z^2} + \left(\frac{\partial^2 w}{\partial x\partial z} \right)^2 \right] + \frac{h_{11}}{a_{33}}\left(z^2 - \frac{h^2}{4} \right)\left[\frac{\partial^3 w}{\partial z^3} + \frac{\partial^2 w}{\partial z^2}\frac{\partial^4 w}{\partial z^4} + \left(\frac{\partial^3 w}{\partial z^3} \right)^2 \right]$$

As seen, Eq. (34) can exactly satisfy the magnetic conditions requested by Eq. (33). Afterwards, by considering the component of the lateral magnetic field only, we have the linearized magnetic field component as presented below

$$
\begin{aligned}
H_z = &-2z\frac{q_{31}}{a_{33}}\frac{\partial^2 u}{\partial x \partial z} - 2z\frac{q_{33}}{a_{33}}\frac{\partial^2 w}{\partial z^2} - 2z\frac{h_{46}}{a_{33}}\left(\frac{\partial^3 u}{\partial x^2 \partial z} + \frac{\partial^3 w}{\partial x^3}\right) - 2z\frac{h_{15}}{a_{33}}\frac{\partial^3 u}{\partial x \partial z^2} - 2z\frac{h_{11}}{a_{33}}\frac{\partial^3 w}{\partial z^3} \\
&+\frac{\psi}{h} + \frac{q_{31}}{a_{33}}\left(\frac{h^2}{4}-z^2\right)\frac{\partial^3 u}{\partial x \partial z^2} + \frac{q_{33}}{a_{33}}\left(\frac{h^2}{4}-z^2\right)\frac{\partial^3 w}{\partial z^3} + \frac{h_{46}}{a_{33}}\left(z^2-\frac{h^2}{4}\right)\left(\frac{\partial^4 u}{\partial x^2 \partial z^2} + \frac{\partial^4 w}{\partial x^3 \partial z}\right) \\
&+\frac{h_{15}}{a_{33}}\left(z^2-\frac{h^2}{4}\right)\frac{\partial^4 u}{\partial x \partial z^3} + \frac{h_{11}}{a_{33}}\left(z^2-\frac{h^2}{4}\right)\frac{\partial^4 w}{\partial z^4}
\end{aligned}
\tag{35}
$$

Finally, after performing lots of mathematical efforts, the bending governing equations can be acquired, linearized, and represented as follows:

$$
\begin{aligned}
&C_{11}\frac{\partial^2 u}{\partial x^2} + (C_{13}+C_{55})\frac{\partial^2 w}{\partial x \partial z} + \frac{h_{46}q_{31}}{a_{33}}\left(z^2-\frac{h^2}{4}\right)\frac{\partial^5 u}{\partial x^3 \partial z^2} + \frac{h_{46}q_{31}}{a_{33}}\left(z^2-\frac{h^2}{4}\right)\frac{\partial^5 w}{\partial x^4 \partial z} \\
&+\left[\frac{q_{31}^2}{a_{33}}\left(\frac{h^2}{4}-z^2\right) + 2\frac{zh_{15}q_{31}+h_{15}^2}{a_{33}} + \frac{1}{2}(g_{15}+g_{26}+g_{66}) + g_{22}+g_{62}+g_{51}\right]\frac{\partial^4 u}{\partial x^2 \partial z^2} \\
&+2\left(\frac{h_{15}q_{31}-zq_{31}^2}{a_{33}}\right)\frac{\partial^3 u}{\partial x^2 \partial z} + \left[\frac{2h_{15}q_{31}}{a_{33}}\left(z^2-\frac{h^2}{4}\right)\right]\frac{\partial^5 u}{\partial x^2 \partial z^3} - \frac{h_{15}h_{11}}{a_{33}}\left(z^2-\frac{h^2}{4}\right)\frac{\partial^6 w}{\partial x \partial z^5} \\
&+2\left(\frac{h_{15}q_{33}-zq_{31}q_{33}}{a_{33}}\right)\frac{\partial^3 w}{\partial x \partial z^2} + \left[g_{52}+\frac{1}{2}(g_{56}+g_{65}+g_{25})\right]\frac{\partial^4 u}{\partial x \partial z^3} + g_{54}\frac{\partial^4 w}{\partial z^4} \\
&+\left[\frac{q_{31}q_{33}}{a_{33}}\left(\frac{h^2}{4}-z^2\right) + \frac{2h_{15}h_{11}+2zh_{11}q_{31}+4zh_{15}q_{33}}{a_{33}} + g_{53}+g_{64}+g_{24}+\frac{g_{55}}{2}\right]\frac{\partial^4 w}{\partial x \partial z^3} \\
&+\left[\frac{h_{11}q_{31}}{a_{33}}\left(z^2-\frac{h^2}{4}\right) - \frac{h_{15}q_{33}}{a_{33}}\left(\frac{h^2}{4}-z^2\right)\right]\frac{\partial^5 w}{\partial x \partial z^4} - \frac{h_{15}^2}{a_{33}}\left(z^2-\frac{h^2}{4}\right)\frac{\partial^6 u}{\partial x^2 \partial z^4} + C_{55}\frac{\partial^2 u}{\partial z^2} \\
&+2\left(\frac{h_{15}h_{46}-zh_{46}q_{31}}{a_{33}}\right)\left(\frac{\partial^4 u}{\partial x^3 \partial z} + \frac{\partial^4 w}{\partial x^4}\right) - \frac{h_{15}h_{46}}{a_{33}}\left(z^2-\frac{h^2}{4}\right)\left(\frac{\partial^6 u}{\partial x^3 \partial z^3} + \frac{\partial^6 w}{\partial x^4 \partial z^2}\right) \\
&+\left(g_{61}+g_{21}+g_{12}+\frac{g_{16}}{2}\right)\frac{\partial^4 u}{\partial x^3 \partial z} + \frac{1}{2}(g_{26}+g_{66}+g_{15}+2g_{13})\frac{\partial^4 w}{\partial x^3 \partial z} + \frac{g_{55}}{2}\frac{\partial^4 u}{\partial z^4} \\
&+g_{11}\frac{\partial^4 u}{\partial x^4} + \frac{g_{16}}{2}\frac{\partial^4 w}{\partial x^4} + \left[g_{63}+g_{14}+g_{23}+\frac{1}{2}(g_{56}+g_{65}+g_{25})\right]\frac{\partial^4 w}{\partial x^2 \partial z^2} = 0
\end{aligned}
\tag{36a}
$$

$$
\begin{aligned}
&\left(C_{33}-2\frac{q_{33}^2}{a_{33}} + q_{33}\frac{\psi}{h}\right)\frac{\partial^2 w}{\partial z^2} + \left[\frac{4h_{11}q_{33}-2zq_{33}^2}{a_{33}} - \frac{z^2 q_{33}^2}{a_{33}}\right]\frac{\partial^3 w}{\partial z^3} + \frac{g_{66}}{2}\frac{\partial^4 w}{\partial x^4} \\
&+\left[\frac{2h_{11}^2+6zh_{11}q_{33}}{a_{33}} + \frac{q_{33}^2}{a_{33}}\left(\frac{h^2}{4}-z^2\right) + g_{44}\right]\frac{\partial^4 w}{\partial z^4} + 2\left[\frac{h_{11}q_{33}}{a_{33}}\left(z^2-\frac{h^2}{4}\right) - \frac{zh_{11}^2}{a_{33}}\right]\frac{\partial^5 w}{\partial z^5} \\
&-\frac{2h_{46}q_{33}}{a_{33}}\left(\frac{\partial^3 u}{\partial x^2 \partial z} + \frac{\partial^3 w}{\partial x^3}\right) + \left[2z\left(\frac{h_{15}q_{33}+h_{11}q_{31}}{a_{33}}\right) + \frac{1}{2}(g_{55}+g_{35}+g_{46}) + g_{42}\right]\frac{\partial^4 u}{\partial x \partial z^3} \\
&+\left[2\frac{h_{11}h_{46}}{a_{33}} + g_{52}+g_{32}+g_{41} + \frac{1}{2}(g_{65}+g_{36}+g_{56})\right]\frac{\partial^4 u}{\partial x^2 \partial z^2} - \frac{h_{11}^2}{a_{33}}\left(z^2-\frac{h^2}{4}\right)\frac{\partial^6 w}{\partial z^6} \\
&+\left(\frac{4h_{11}q_{31}-2h_{15}q_{33}-zq_{31}q_{33}}{a_{33}}\right)\frac{\partial^3 u}{\partial x \partial z^2} + \left[\frac{2h_{11}h_{46}}{a_{33}} + \frac{1}{2}(g_{65}+g_{36}+g_{56}) + g_{63}\right]\frac{\partial^4 w}{\partial x^3 \partial z} \\
&+\left[\frac{h_{15}q_{33}}{a_{33}}\left(z^2-\frac{h^2}{4}\right) - \frac{2zh_{11}h_{15}}{a_{33}} - \frac{h_{11}q_{31}}{a_{33}}\left(\frac{h^2}{4}-z^2\right)\right]\frac{\partial^5 u}{\partial x \partial z^4} + C_{55}\frac{\partial^2 w}{\partial x^2} + N_{xx}\frac{\partial^2 w}{\partial x^2} \\
&+\frac{h_{46}q_{33}}{a_{33}}\left(z^2-\frac{h^2}{4}\right)\frac{\partial^5 u}{\partial x^2 \partial z^3} + \left(C_{55}+C_{13} - \frac{2q_{31}q_{33}}{a_{33}}\right)\frac{\partial^2 u}{\partial x \partial z} + \left(\frac{2h_{11}q_{31}-2zq_{31}q_{33}}{a_{33}}\right)\frac{\partial^3 u}{\partial x \partial z^2} \\
&-\frac{2zh_{11}h_{46}}{a_{33}}\left(\frac{\partial^5 u}{\partial x^2 \partial z^3} + \frac{\partial^5 w}{\partial x^3 \partial z^2}\right) + \left[\frac{2h_{11}h_{15}+4zh_{11}q_{31}-2zh_{15}q_{33}}{a_{33}} + \frac{q_{31}q_{33}}{a_{33}}\left(\frac{h^2}{4}-z^2\right)\right]\frac{\partial^4 u}{\partial x \partial z^3} \\
&-\frac{h_{11}h_{46}}{a_{33}}\left(z^2-\frac{h^2}{4}\right)\left(\frac{\partial^6 u}{\partial x^2 \partial z^4} + \frac{\partial^6 w}{\partial x^3 \partial z^3}\right) - \frac{h_{11}h_{15}}{a_{33}}\left(z^2-\frac{h^2}{4}\right)\frac{\partial^6 u}{\partial x \partial z^5} + \frac{h_{46}q_{33}}{a_{33}}\left(z^2-\frac{h^2}{4}\right)\frac{\partial^5 w}{\partial x^3 \partial z^2} \\
&+g_{61}\frac{\partial^4 u}{\partial x^4} + \left(g_{62}+g_{51}+g_{31}+\frac{g_{66}}{2}\right)\frac{\partial^4 u}{\partial x^3 \partial z} + \left[g_{64}+g_{33}+g_{53}+\frac{1}{2}(g_{55}+g_{35}+g_{46})\right]\frac{\partial^4 w}{\partial x^2 \partial z^2} \\
&+(g_{54}+g_{34})\frac{\partial^4 w}{\partial x \partial z^3} + \left(g_{43}+\frac{g_{45}}{2}\right)\frac{\partial^4 w}{\partial x \partial z^3} + \frac{g_{45}}{2}\frac{\partial^4 u}{\partial z^4} = 0
\end{aligned}
\tag{36b}
$$

The above-presented equations predict the linear bending response of a 3D piezomagnetic-flexomagnetic beam.

3. Solution technique

Semi-analytical solution methods are a set of methods and techniques that can be used to solve mathematical and physical problems explicitly and reach a mathematical and workable solution. For example, one of the semi-analytical methods is the SAPM [Dastjerdi & Akgöz, 2019; Dastjerdi et al., 2020a, Sh. 2020b, Sh. 2021c, 2022a, Sh. 2022b, 2023a, 2023b], which provides the possibility of solving the problem faster and easier by using the decomposition of functions into a set of simpler polynomial functions. Due to its high precision and accuracy, this method has been used recently to solve physical problems. In the onward, the 3D version of the SAMP method for 3D problems will be in use. The details for the SAPM method are available in the former works [Dastjerdi & Akgöz, 2019; Dastjerdi et al., 2020a, Sh. 2020b, Sh. 2021c, 2022a, Sh. 2022b, 2023a, 2023b].

The linear sixth-order partial differential equations have been derived and illustrated by Eq. (36). To ensure that the solution technique can provide appropriate numerical results, one must ensure the satisfaction of boundary conditions. The derived differential equations can be resolved based on the following expressed geometrical (essential) and natural (force) boundary conditions enforced at both ends and top and bottom surfaces of the beam,

- Clamped (C):

$$u|_{x=0,L} = w|_{x=0,L} = 0$$

- Simply-supported (S):

$$w|_{x=0,L} = 0, \sigma_{xx}|_{x=0,L} = N_{xx}$$

- Free (F):

$$\sigma_{xx}|_{x=0,L} = N_{xx}, \tau_{xz}|_{z=-\frac{h}{2},+\frac{h}{2}} = 0$$

The boundary conditions at the top and bottom surfaces of the beam are expressed as follows:

Top: $\sigma_{zz}|_{z=-\frac{h}{2},+\frac{h}{2}} = Q, \tau_{xz}|_{z=-\frac{h}{2},+\frac{h}{2}} = 0$, where $Q = q/b$.

Bottom: $\sigma_{zz}|_{z=-\frac{h}{2},+\frac{h}{2}} = \tau_{xz}|_{z=-\frac{h}{2},+\frac{h}{2}} = 0$

Having available the appropriate and previously utilized allowable boundary condition expressions [Dastjerdi & Akgöz, 2019; Dastjerdi et al., 2020a, Sh. 2020b, Sh. 2021c, 2022a, Sh. 2022b, 2023a, 2023b], one can have

$$u(x,z) = \sum_{i=1}^{N} \sum_{j=1}^{M} p_{(j+M(i-1))} x^{(i-1)} z^{(j-1)} \tag{37a}$$

$$w(x,z) = \sum_{i=1}^{N} \sum_{j=1}^{M} p_{(j+M(i-1)+M.N)} x^{(i-1)} z^{(j-1)} \tag{37b}$$

where N and M are distributions of points on the beam thickness.

To impose the SAPM technique, initially, the media will be divided by grid points. The points mesh here for x and z coordinates concerning Eq. (37) follows the well-used Chebyshev-Gauss-Lobatto (CGL) grid points as

$$x_i = \frac{1}{2}L\left(1 - \cos\frac{i-1}{N-1}\pi\right), i = 1, 2, \dots, N \tag{38a}$$

$$z_k = \frac{1}{2}h\left(1 - \cos\frac{i-1}{M-1}\pi\right), k = 1, 2, \dots, M \tag{38b}$$

The CGL is pictured by Fig. 2. On the domain, each point is able to move and hence, thickness stretching as a 3D deformation elasticity property can also be achieved. The solid red points represent the governing equations and the solid black ones obey the boundaries. This kind of grid points differs with the simple one. It actually gives non-equal distance points and is further accurate than the simple grid points due to the boundaries points that are nearer to one another.

As far as there are two unknown parameters (u and w) for each point,

$$u = [u(x_1,z_1), \dots, u(x_N,z_1), u(x_1,z_2), \dots, u(x_N,z_2), \dots, u(x_1,z_M), \dots, u(x_N,z_M)]^T \tag{39a}$$
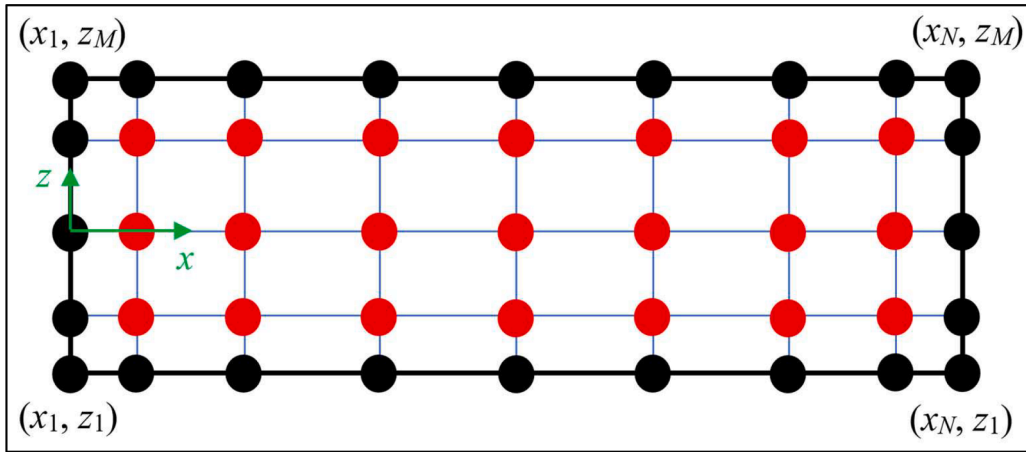
Fig. 2. CGL grid points for a symmetrical beam ($N = 9$, $M = 5$).

$$w = [w(x_1, z_1), ..., w(x_N, z_1), w(x_1, z_2), ..., w(x_N, z_2), ..., w(x_1, z_M), ..., w(x_N, z_M)]^T \qquad (39b)$$

Then, there will be $N \times M \times 2$ equations number and the same unknown. Later, the Newton-Raphson technique aids us in computing the u and w values for unknown points by finding the answer to the algebraic equations.

4. Results comparison

Since the current solution is based on a semi-analytical method, which itself is based on polynomial functions, we must check the convergence of the results at the beginning of the results section. In fact, we should know how many nodes along the length and thickness of the beam will converge our results with the help of this solution method. Then, considering the number of converged points, the main results can be extracted.

With the help of the figures presented in this part, i.e. in Figs. 3a and 3b, the convergence of the results under different boundary conditions is shown. It should be noted that both figures are a problem for a thick macrobeam regardless of the magnetization part. As shown in Fig. 3a, for the clamped-clamped (C–C) and clamped-simply supported (C–S) boundary conditions, the results are converged at the number of nodes 13 in both thickness and length directions. But it is clear from Fig. 3b that in the boundary condition of clamped-free edges (C-F), the convergence of the results will be after the number 13. In fact, this means that the free boundary condition in the utilized semi-analytical method requires larger number of polynomials to give correct structural behavior and is almost a more sensitive condition.

In the discussion of engineering and numerical problems, it is always customary to validate the derived mathematical model with those of the available references and evaluate its accuracy so that the correctness of the results can be ensured before an in-depth investigation of the mechanical behavior of the structure. This goal will be possible through Figs. 4a, 4b, and 5a, 5b.
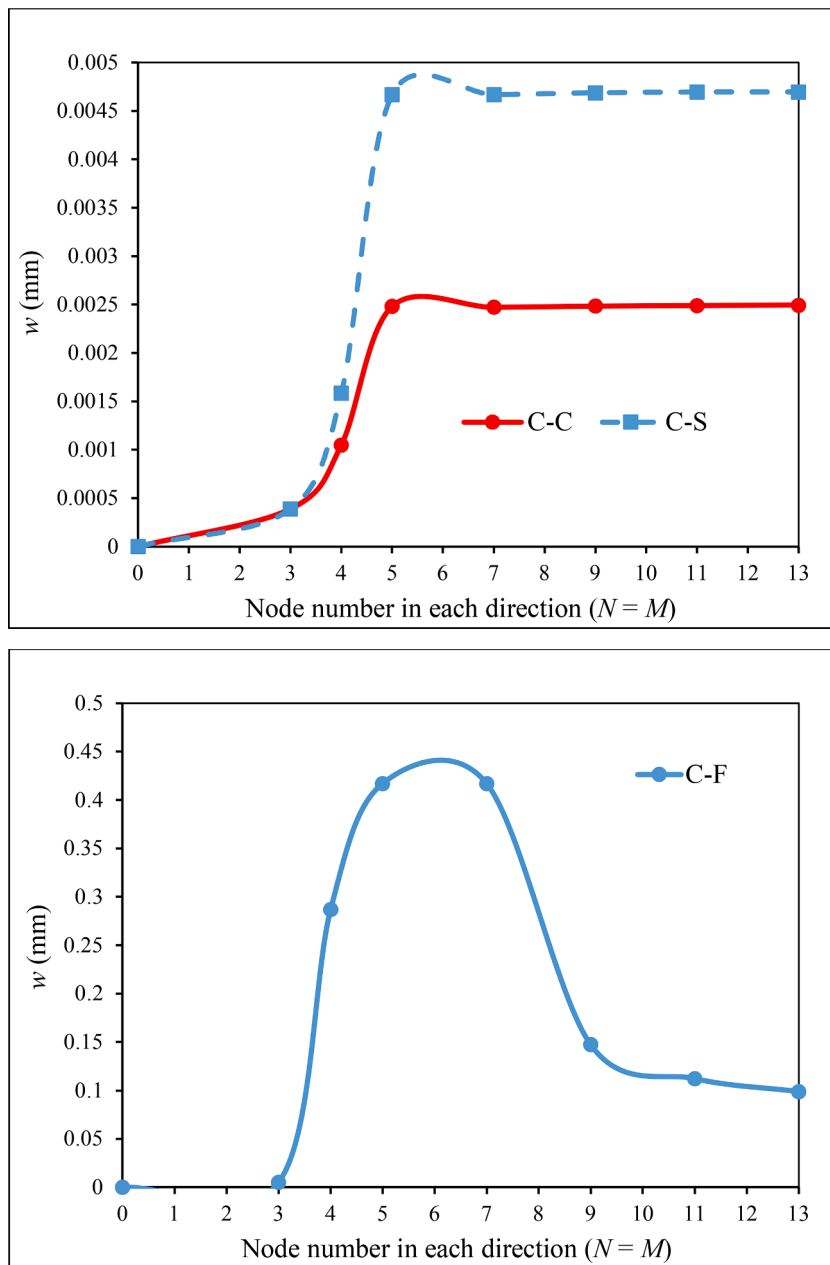
Figs. 4a, 4b, and 5a, 5b compare the bending results for a thick macrobeam assuming zero values for all intelligent parameters. The comparison is done between the results of the current model and the finite element numerical method. In Figs. 4a and 4b, the beam is limited in the clamped-free states, while in Figs. 5a and 5b, it is evaluated for the beam with two clamped ends. As it is firmed up by these figures, the maximum transverse deflections in both compared examples wholly and clearly serve to prove that the presently derived model and the solution process are highly accurate.

5. Results presentation

The previous section has fully and error-freely verified the solution method and the present computational model with the help of existing references. In this section, we are evaluating the important parameters of the problem in detail. To extract the mechanical and magnetic properties of the piezo-flexomagnetic beam (PFM) model, some literature is used for the present results in the discussion of three-dimensional elasticity. Due to the lack of enough literature and studies, we here consider the values of the reverse FM parameters equal to the direct ones. Also, the piezomagnetic parameters' amounts and elasticity constants are taken from [Gholami & Ansari, 2017; Malikan & Nguyen, 2018; Sidhardh & Ray, 2018; Kuo & Wang, 2022] for a $CoFe_2O_4$ material. Hereafter, if any parameter is not mentioned in the title of the figures, that means the value is the default one. In the next section, in order to facilitate and simplify the discussion of the results, the effects of vital parameters will be presented in sub-sections.

5.1. Slenderness effect

One of the most important issues that can be investigated in the three-dimensional elasticity analysis of beams and plates is the issue of large deformations. In the topic of beam and plate theories, even higher-order theories such as Reddy plate theory, the deformations
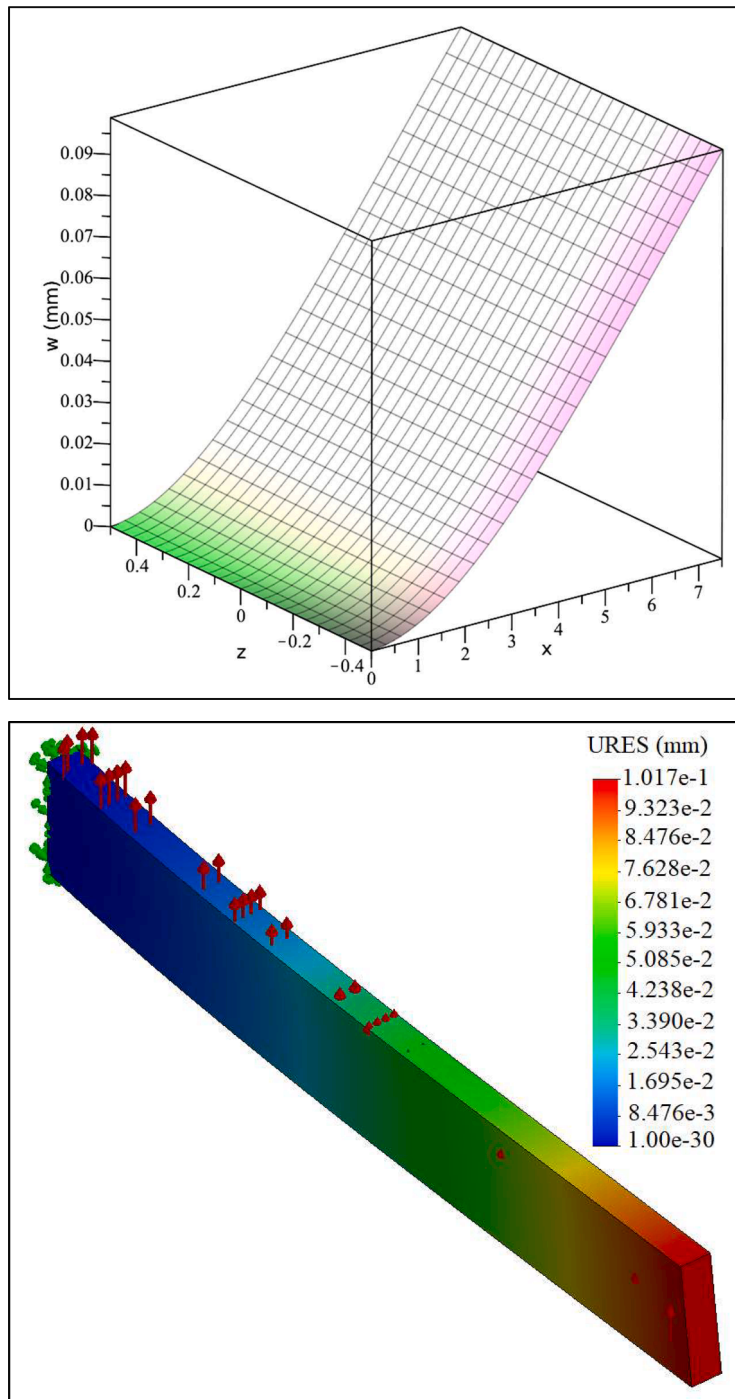
Fig. 3. a Mesh convergence in the SAPM ($L/h = 7.5$, $b/h = 0.25$, $E = 190$ GPa, $\nu=0.29$, $Q = 1$ kPa).
b Mesh convergence in the SAPM ($L/h = 7.5$, $b/h = 0.25$, $E = 190$ GPa, $\nu=0.29$, $Q = 1$ kPa).

are absolutely small, but the displacements may be small or large. In the physics of nature, deformations are often large. Therefore, with the help of three-dimensional elasticity, the flexomagnetic beam can be analyzed closer to its exact physics.
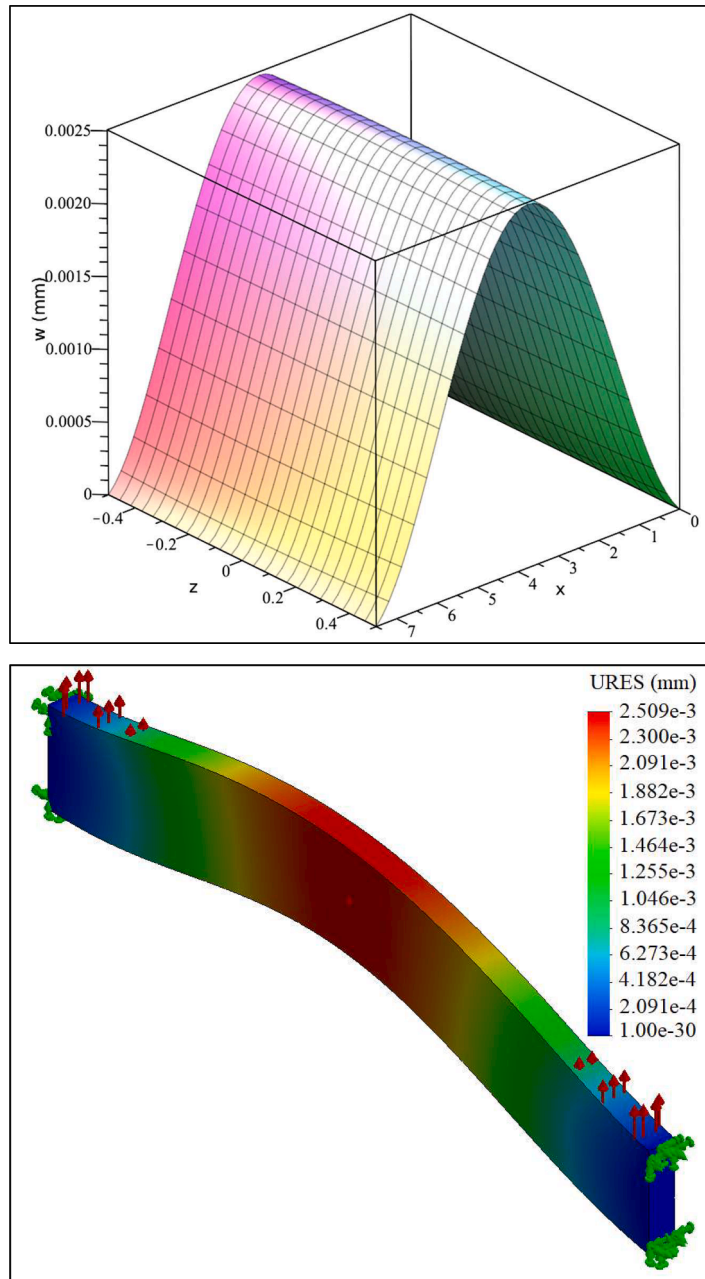
Fig. 6 is one of the most critical results of this study for a PFM. The figure has been assumed to show changes in the deformation in two directions. The first direction is the longitudinal direction that is usually presented in the one-dimensional analysis of the PFM beam to indicate deflections, which shows the maximum deflection here too. Anyway, the elastic changes along the thickness are assumed to be constant in beam and plate theories, and here these changes are considered inside the problem. As one sees, when the thick smart beam bends under the transverse load, not only the deflection but also the deformation occurs in the thickness of the beam. It is the large deformations that become significant for the problems of thick PFM beams and sheets.

Another worthwhile result earned from Fig. 6 is seen in boundaries. In a normal situation and for thin or moderately thick domains, deformation in a clamped boundary is encountered with a low slope and then a steep one. Nevertheless, in a very thick structure and small deflections, the case is non-identical.

Fig. 4. a 3D results for C-F ($L/h = 7.5$, $b/h = 0.25$, $E = 190$ GPa, ν=0.29, $Q = 1$ kPa).
b FEM results for C-F ($L/h = 7.5$, $b/h = 0.25$, $E = 190$ GPa, ν=0.29, $Q = 1$ kPa).

The results obtained in Fig. 6 can be further investigated and expanded. By presenting Figs. 7a, 7b, and 7c, the effect of the slenderness ratio of the beam from a very thin beam to a very thick one has been examined. It should be mentioned that for Fig. 7a, the vertical axis of the diagram is for w_s parameter, which is the ratio of the deflection for the lowest surface of the thickness to the highest surface. The lower value of this parameter shows that the deformation of the beam increases through the thickness. In very thin beams, the beam has no deformation along the thickness and the amount of the w_s parameter equals one. That is, the deflection is constant in line with the thickness. With the help of the figure, it is clear that as the beam becomes thicker, the changes in thickness go up.

14

Fig. 5. **a** 3D results for C–C ($L/h = 7.5$, $b/h = 0.25$, $E = 190$ GPa, $\nu=0.29$, $Q = 1$ kPa).
b FEM results for C–C ($L/h = 7.5$, $b/h = 0.25$, $E = 190$ GPa, $\nu=0.29$, $Q = 1$ kPa).

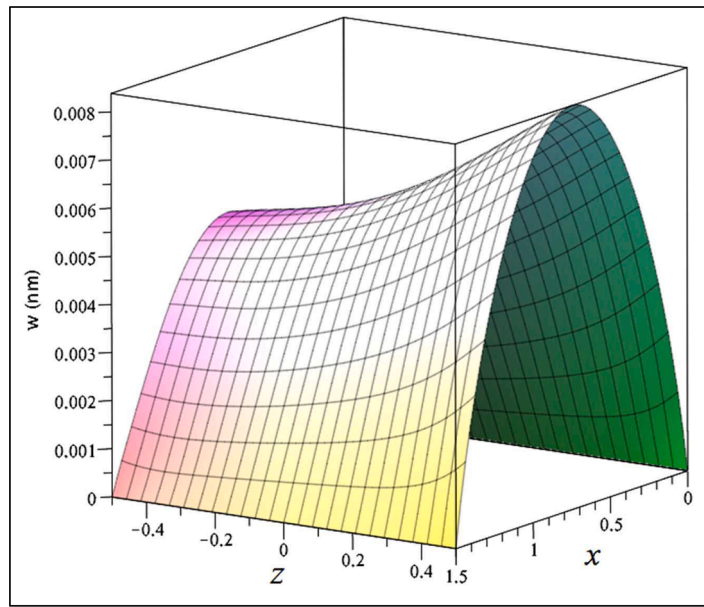**Fig. 6.** Deflection vs. thickness deformation ($L/h = 1.5$, $b/h = 0.05$, $Q = 0.1$ Pa, $l/h = 0.1$, $\psi=0$, C–C).

Moreover, another important result that can be pulled out from this figure is that as the beam gets thicker, the slight difference in the results of the two curves seen at the beginning increases fundamentally later. The first curve is related to a non-intelligent micro/nanobeam and the second one is the smart micro/nanobeam. When smart parameters enter the problem, they affect the change and deformation of the thickness. This effect is reduced to a greater difference in the upper and lower layers of the thickness while adding smartness. Such a result doubles the importance of 3D elasticity analysis for smart beams.

Furthermore, Fig. 7b extends the thickness deformation studies in Fig. 7a by a change in the width of the beam. Apparently, the increase or decrease in the width dimension of the beam influences the w_s values, and this outcome determines that the third dimension of the beam, namely width, is straightly related to the way that thickness deforms.

$$w_s = \frac{Deflection\ of\ the\ lowest\ thickness\ surface}{Deflection\ of\ the\ highest\ thickness\ surface} \tag{39}$$
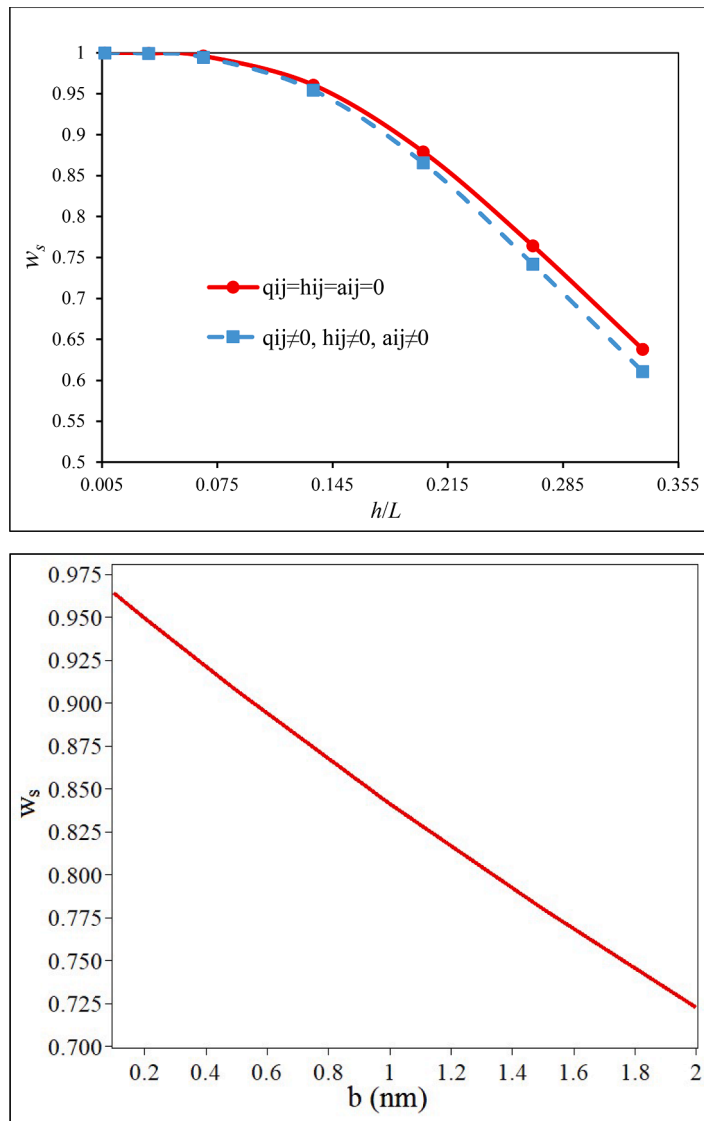
Fig. 7c examines another parameter versus the slenderness factor of the beam. The mentioned parameter is w_d, which is the ratio of three-dimensional deflection to that of one-dimensional for smart and non-smart micro/nanobeams. At the beginning of the results and the direction of the very thin beam, one can see the biggest difference between the two smart and non-smart beams. But this difference gradually decreases and increases again after a certain amount of thickness-to-length ratio. As seen, as the beam becomes thicker in both intelligent and non-intelligent modes, the value of the w_d parameter also increases, which illustrates that the results of the one-dimensional analysis can be completely rejected in thick beams. More importantly, this diagram displays that for the analysis of smart micro/nanobeams, even in very small thicknesses, the one-dimensional analysis does not provide appropriate and correct results.

$$w_d = \frac{Deflection\ of\ 3D\ beam}{Deflection\ of\ 1D\ beam} \tag{40}$$

5.2. Strain gradient parameter effect

The strain gradient parameter (l) is decisive in analyzing the mechanical behavior of micro- and nanostructures. But this importance will be multiplied when the strain gradient becomes inclined to create the flexomagnetic effect. By presenting Figs. 8a, 8b, and 8c, the significance of the strain gradient parameter has been proven. In all three figures, the longitudinal axis is shown for the deflections in line with the length, and the transverse axis demonstrates the deflection variations in the thickness direction (deformations). The boundary conditions in all three diagrams have been investigated completely fixed for two ends. The input parameters of the problem can be seen in the titles of the figures, and it should be noted that the value of the magnetic potential is based on milliamperes. It is noteworthy that the transverse load has been neglected in all three figures and the deflections and deformations

16

Fig. 7. a Thickness deformations vs. slenderness ratio ($b/h = 0.05$, $Q = 0.1$ Pa, $l/L = 1/15$, ψ=0, C–C).
b Thickness deformations vs. changes in the width of the beam ($L/h = 5$, $l/h = 0.025$, $Q = 1$ Pa, ψ=2 mA, C–C).
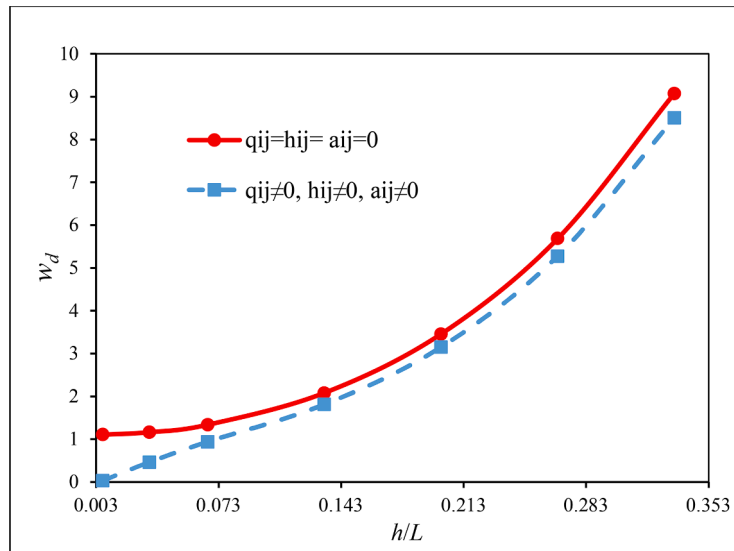**c** 3D elasticity effect vs. slenderness ratio ($b/h = 0.05$, $Q = 0.1$ Pa, $l = 0$, ψ=0, C–C).
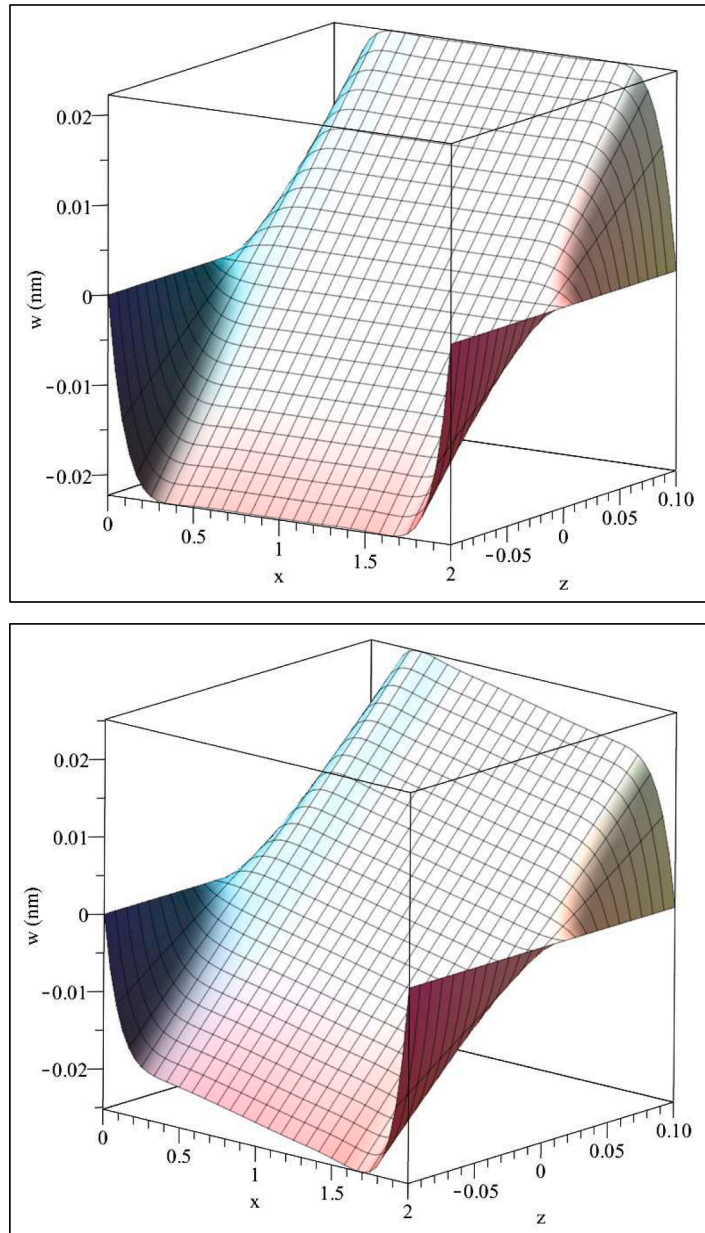
Fig. 7. (*continued*).

are the result of the magnetic potential and the strain gradient parameter only. In fact, the reason for omitting the transverse load is to show the pure deformations originated from strain gradients and the magnetic field. In the figures, the values of the strain gradient parameter have been selected as zero, one-tenth, and two-tenth of the thickness, respectively. The most momentous results that can be drawn from these three figures are that changes in the strain gradient parameter not only affect the deflection of the beam (Note that if the maximum deflection here is not in the center of the length that is because the transverse static load has not been imposed) but also lead to deformation in the thickness of the beam.

In addition to this, in one-dimensional analysis, when the lateral load exists, the maximum deflection occurs in the longitudinal center of the beam; however, when the force is eliminated, there is no deflection even if the strain gradient and magnetic force are involved inside the equations [Malikan & Eremeyev, 2020c]. But, according to these figures, in 3D analysis, even if there is no static bending transverse load, the magnetic force makes a deflection and the strain gradient also affects the deflection. This finding cannot be obtained utilizing a 1D elasticity analysis. Pursuant to the research background, increasing the value of the strain gradient parameter leads to increased stiffness of the material and a decrease in the beam's deflection. The comparison of the three figures reveals that in the three-dimensional analysis of the smart beams, the effect of the strain gradient causes different values of deflections along with the length. All in all, the noteworthiness of 3D analysis here manifests that the essence of the strain gradients, in addition to influencing the deflection, happens other things on the beam, and the strain gradient causes the beam's twisted form along its length as well.

The results harvested from the effective parameter of strain gradient will not be limited to the previous figures, and by bringing forward Fig. 9, another interesting result can be witnessed. This figure represents the variations in the numerical value of the strain gradient parameter compared to the changes in the w_s parameter. This parameter has been explained earlier. The importance of collecting the results in this figure is to show how the increase in the value of the strain gradient parameter has an effect on the thickness deformation. Fig. 9 conveys that when the strain gradient parameter is left out of the analysis, the dissimilarity in the deflection of the bottom and top layers of the thickness looks small. Regardless of how, increasing the value of the strain gradient parameter results in a major deviation of the deflection values at the highest and lowest levels of the beam thickness. The meaning of this achievement is that the strain gradient has an enormous effect on the beam structure and finally, at large values of the strain gradient parameter, considerable deformation occurs in the thickness of the beam.

5.3. Magnetic potential effect

The effect of changes in the magnetic potential parameter resulting from the external magnetic field can be indicated in Fig. 10. The unit of magnetic potential is the milliampere. As one can see, when the magnetic potential has zero value and as if there is no external magnetic field, the changes in thickness deformation or the deflection ratio of different thickness layers are insignificant. However, as

Fig. 8. a Deflections vs. strain gradient effect ($L/h = 10$, $b/h = 0.5$, $Q = 0$, $l/h = 0$, ψ=20 mA, C–C).
b Deflections vs. strain gradient effect ($L/h = 10$, $b/h = 0.5$, $Q = 0$, $l/h = 0.1$, ψ=20 mA, C–C).
c Deflections vs. strain gradient effect ($L/h = 10$, $b/h = 0.5$, $Q = 0$, $l/h = 0.2$, ψ=20 mA, C–C).

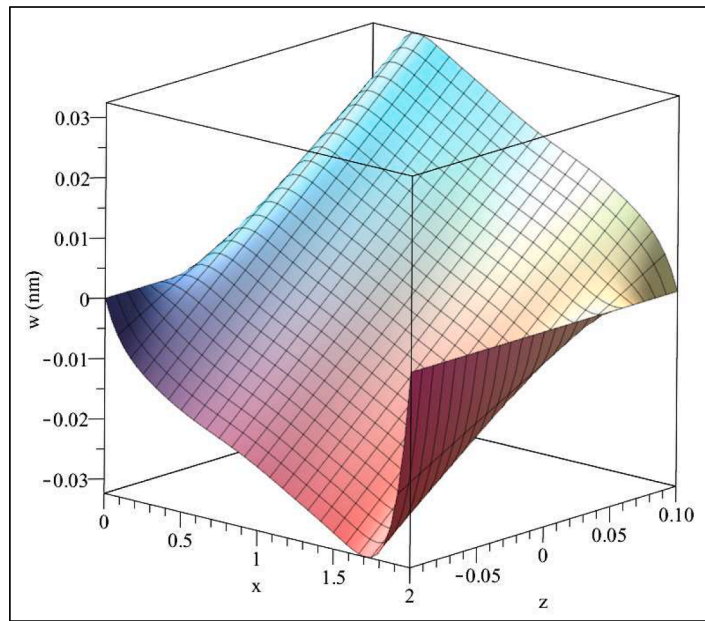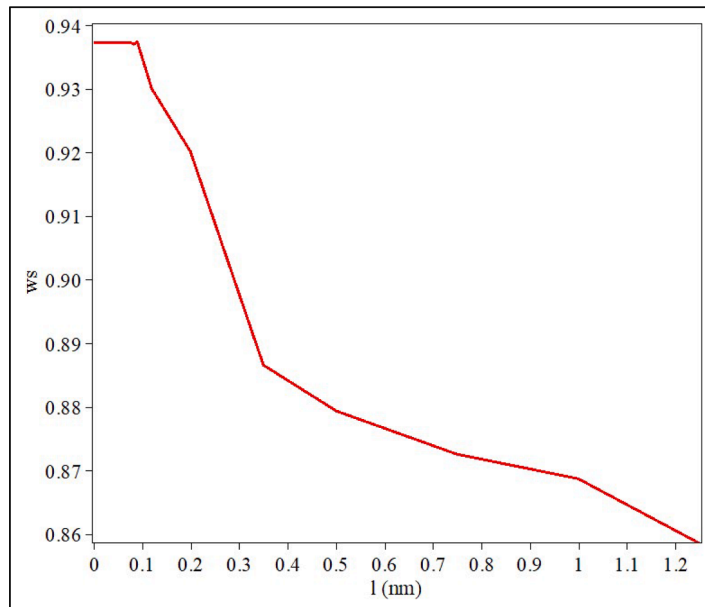**Fig. 8.** (*continued*).

Fig. 9. W_s parameter vs. strain gradient effect ($L/h = 10$, $b/h = 0.5$, $Q = 1$ Pa, ψ=20 mA, C–C).
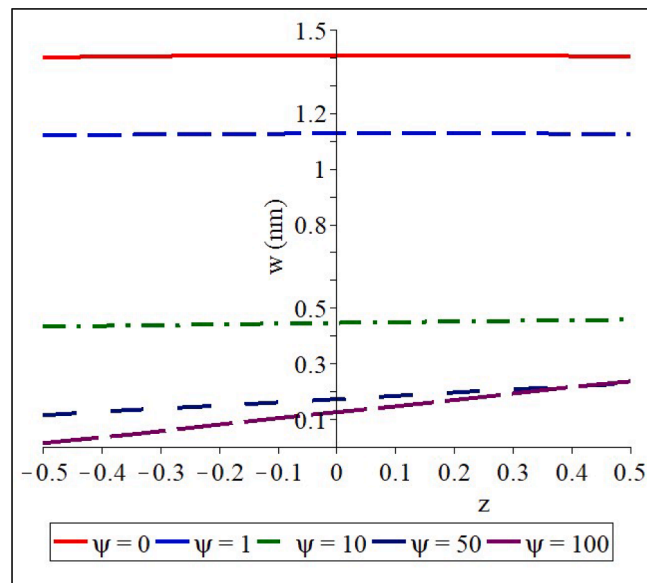
20

Fig. 10. Deflections vs. magnetic potential parameter (mA) ($L/h = 10$, $b/h = 0.5$, $Q = 1$ Pa, $l/h = 0.1$, C–C).

soon as the external magnetic field is applied and the magnetic potential has a value, the deflection in different layers of thickness will have different values, so that when the amount of the magnetic potential is large enough, the deflection difference in the upper and lower layers of thickness will be remarkable, and principally, the thickness deformation is substantial.

6. Conclusion

With the aim of identifying the effect of flexomagneticity (FM) in a three-dimensional mechanical analysis, a parametric study has been conducted through a case study. To the best of our knowledge and upon reviewing the literature, it was crystal clear that a three-dimensional (3D) elasticity study of the smart flexomagnetic composite structure was not evaluated prior to this study. Thus, a further investigation was seriously needed. To manage such an analysis, the governing equations incorporated the thickness stretching effect, which means the term $\partial/\partial z$. A proposed flexomagnetic model that was restricted to piezomagnetic structures has been re-utilized. Using the variational technique, the governing equations were derived for a thick composite beam by adjusting and compiling several approaches, which were composed of a 3D beam kinematic model, von Kármán strain nonlinearity, Hamilton's principle, and appointed direct and converse FM models. The essential tensors were given in 3D forms with respect to the 3D study. Thereafter, the derived characteristic linear three-dimensional bending equations were transferred to a 3D semi-analytical Polynomial Method to propagate numerical results. This work highlighted the importance of 3D mechanical analyses on the multi-physic connection, such as flexomagneticity, and filled a gap by revealing new insights on FM. Although some findings are pointed out and listed below, the novel achievements are not limited to these,

- In 1D analysis of small-scale smart beams, when the external loads are applied, the presence of the strain gradients only induces further material stiffness, but in 3D evaluation, it also affects thickness deformation and beam twisting. The result is physically logical cause the strain gradient means the rate of changes in strains. Thus, while the transverse strain is engaged inside the problem, the strain gradients are more fruitful and have a further impact on the elastic behavior.
- In contrast to the non-smart structures, the smart feature brings about further deformations inside the thickness and consequently, the 3D analysis is crucial for smart micro/nanocomposite structures.
- 3D evaluations displayed that the magnetic field influences not only the beam's deflections but the beam's deformations as well.
- In 1D investigations of small-scale smart structures, if the static bending load is removed, the beam will not confront any deflection even if the other higher-order and external factors like magnetic influence are engaged in the problem. However, in 3D studies, it was shown that some parameters, such as magnetic potential can affect the deflection and deformation of the structure no matter whether the lateral load is forced.

CRediT authorship contribution statement

Mohammad Malikan: Conceptualization, Methodology, Mathematical Modelling, Formal analysis, Investigation, Writing–original draft, Resources, Data curation, Writing–review & editing, Supervision, Project administration, Funding acquisition. **Shahriar Dastjerdi**: Software, Solution, Validation, Visualization, Formal analysis, Investigation, Writing–review & editing. **Victor A. Eremeyev**: Methodology, Formal analysis, Investigation, Writing–review & editing, Supervision, Project administration. **Hamid M.**

Sedighi: Investigation, Data curation, Writing – review & editing.

Declaration of Competing Interest

There is no conflict of interest to disclose regarding manuscript "**On a 3D material modeling of smart nanocomposite structures**" submitted by Mohammad Malikan to International Journal of Engineering Science.

Data availability

The data/code is a part of the authors' future studies and cannot be shared.

References

Abouelregal, A. E., Sedighi, H. M., Faghidian, S. A., & Shirazi, A. H. (2021). Temperature-dependent physical characterisitcs of the rotating nonlocal nanobeams subject to a varying heat source and a dynamic load. *Facta Universitatis, Series: Mechanical Engineering, 19*, 633–656.

Alshenawy, R., Sahmani, S., Safaei, B., Elmoghazy, Y., Al-Alwan, A., & Al Nuwairan, M. (2023). Three-dimensional nonlinear stability analysis of axial-thermal-electrical loaded FG piezoelectric microshells via MKM strain gradient formulations. *Applied Mathematics and Computation, 439*, Article 127623. Article.

Auffray, N., Le Quang, H., & He, Q. C. (2013). Matrix representations for 3D strain-gradient elasticity. *Journal of the Mechanics and Physics of Solids, 61*, 1202–1223.

Borkar, H., Gaikwad, V. M., Choudhary, R. J., Tomar, M., Gupta, V., & Kumar, A (2022). Flexomagnetic effects on inhomogeneously strained multiferroics composites. *Journal of Magnetism and Magnetic Materials, 553*, Article 169274. Article.

Dastjerdi, Sh., & Akgöz, B. (2018). New static and dynamic analyses of macro and nano FGM plates using exact three-dimensional elasticity in thermal environment. *Composite Structures, 192*, 626–641.

Dastjerdi, Sh., & Akgöz, B. (2019). On the statics of fullerene structures. *International Journal of Engineering Science, 142*, 125–144.

Dastjerdi, Sh., Akgöz, B., & Civalek, Ö. (2020a). On the effect of viscoelasticity on behavior of gyroscopes. *International Journal of Engineering Science, 149*, Article 103236. Article.

Dastjerdi, Sh., Akgöz, B., Civalek, Ö., Malikan, M., & Eremeyev, V. A. (2020b). On the non-linear dynamics of torus-shaped and cylindrical shell structures. *International Journal of Engineering Science, 156*, Article 103371. Article.

Dastjerdi, Sh., Akgöz, B., & Civalek, Ö. (2021b). On the shell model for human eye in Glaucoma disease. *International Journal of Engineering Science, 158*, Article 103414. Article.

Dastjerdi, Sh., Alibakhshi, A., Akgöz, B., & Civalek, Ö. (2023a). On a comprehensive analysis for mechanical problems of spherical structures. *International Journal of Engineering Science, 183*, Article 103796. Article.

Dastjerdi, Sh., Civalek, Ö., Malikan, M., & Akgöz, B. (2023b). On analysis of nanocomposite conical structures. *International Journal of Engineering Science, 191*, Article 103918. Article.

Dastjerdi, Sh., & Jabbarzadeh, M. (2017). Non-linear bending analysis of multi-layer orthotropic annular/circular graphene sheets embedded in elastic matrix in thermal environment based on non-local elasticity theory. *Applied Mathematical Modelling, 41*, 83–101.

Dastjerdi, Sh., Malikan, M., Akgöz, B., Civalek, Ö., Wiczenbach, T., & Eremeyev, V. A. (2022a). On the deformation and frequency analyses of SARS-CoV-2 at nanoscale. *International Journal of Engineering Science, 170*, Article 103604. Article.

Dastjerdi, Sh., Malikan, M., Dimitri, R., & Tornabene, F. (2021a). Nonlocal elasticity analysis of moderately thick porous functionally graded plates in a hygro-thermal environment. *Composite Structures, 255*, Article 112925. Article.

Dastjerdi, Sh., Malikan, M., & Tadi Beni, Y. (2022b). A comprehensive study on nonlinear hygro-thermo-mechanical analysis of thick functionally graded porous rotating disk based on two quasi-three-dimensional theories. *Mechanics Based Design of Structures and Machines, 50*, 3596–3625.

Dastjerdi, Sh., Naeijian, F., Akgöz, B., & Civalek, Ö. (2021c). On the mechanical analysis of microcrystalline cellulose sheets. *International Journal of Engineering Science, 166*, Article 103500. Article.

Eliseev, E. A., Glinchuk, M. D., Khist, V., Skorokhod, V. V., Blinc, R., & Morozovska, A. N (2011). Linear magnetoelectric coupling and ferroelectricity induced by the flexomagnetic effect in ferroics. *Physical Review B, 84*, Article 174112. Article.

Eliseev, E. A., Morozovska, A. N., Glinchuk, M. D., & Blinc, R (2009). Spontaneous flexoelectric/flexomagnetic effect in nanoferroics. *Physical Review B, 79*, Article 165433. Article.

Eliseev, E. A., Morozovska, A. N., Khist, V. V., & Polinger, V (2019). Chapter Six - Effective flexoelectric and flexomagnetic response of ferroics, Editor(s): Robert L. Stamps, Helmut Schultheiß. *Solid State Physics, Academic Pre, 70*, 237–289.

Ezzin, H., Mkaoir, M., Qian, Z., Arefi, M., & Das, R (2022). Lamb Wave Analysis in Anisotropic Multilayer Piezoelectric-piezomagnetic Material. *Journal of Applied and Computational Mechanics, 8*, 629–640.

Fattahi, I., & Mirdamadi, H. R. (2017). Novel composite finite element model for piezoelectric energy harvesters based on 3D beam kinematics. *Composite Structures, 179*, 161–171.

Gholami, R., & Ansari, R. (2017). A unified nonlocal nonlinear higher-order shear deformable plate model for postbuckling analysis of piezoelectric-piezomagnetic rectangular nanoplates with various edge supports. *Composite Structures, 166*, 202–218.

Gia Phi, B., Van Hieu, D., Sedighi, H. M., & Sofiyev, A. H (2022). Size-dependent nonlinear vibration of functionally graded composite micro-beams reinforced by carbon nanotubes with piezoelectric layers in thermal environments. *Acta Mechanica, 233*, 2249–2270.

Gusev, A. A., & Lurie, S. A. (2017). Symmetry conditions in strain gradient elasticity. *Mathematics and Mechanics of Solids, 22*, 683–691.

Hong Lee, J., Kim, K. E., Jang, B. K., Ünal, A. A., Valencia, S., Kronast, F., Ko, K.-T., Kowarik, S., Seidel, J., & Yang, Ch.-H (2017). Strain-gradient-induced magnetic anisotropy in straight-stripe mixed-phase bismuth ferrites: Insight into flexomagnetism. *Physical Review B, 96*, Article 064402. Article.

Jankowski, P (2022). Detection of nonlocal calibration parameters and range interaction for dynamics of FGM porous nanobeams under electro-mechanical loads. *Facta Universitatis, Series: Mechanical Engineering, 20*, 457–478.

M. Malikan et al. *International Journal of Engineering Science 193 (2023) 103966*

Kabychenkov, A. F., & Lisovskii, F. V (2019). Flexomagnetic and flexoantiferromagnetic effects in centrosymmetric antiferromagnetic materials. *Technical Physics, 64*, 980–983.

Karami, B., Janghorban, M., & Fahham, H. (2022). On the stress analysis of anisotropic curved panels. *International Journal of Engineering Science, 172*, Article 103625. Article.

Karami, B., & Ghayesh, M. H. (2023). Vibration characteristics of sandwich microshells with porous functionally graded face sheets. *International Journal of Engineering Science, 189*, Article 103884. Article.

Khabisi-Momeni, H., & Tahani, M. (2022). A size-dependent study on buckling and post-buckling behavior of imperfect piezo-flexomagnetic nano-plate strips. *Advances in nano research, 12*, 427–440.

Kuo, H. Y., & Wang, Y. H. (2022). Wave motion of magneto-electro-elastic laminated plates with membrane-type interfacial imperfections. *Composite Structures, 293*, Article 115661. Article.

Liew, K. M., & Yang, B. (1999). Three-dimensional elasticity solutions for free vibrations of circular plates: A polynomials-Ritz analysis. *Computer Methods in Applied Mechanics and Engineering, 175*, 189–201.

Lukashev, P., & Sabirianov, R. F (2010). Flexomagnetic effect in frustrated triangular magnetic structures. *Physical Review B, 82*, Article 094417. Article.

Makushko, P., Kosub, T., Pylypovskyi, O. V., et al. (2022). Flexomagnetism and vertically graded Néel temperature of antiferromagnetic Cr_2O_3 thin films. *Nature Communications, 13*, 6745. Article.

Malikan, M., & Eremeyev, V. A. (2020a). Free vibration of flexomagnetic nanostructured tubes based on stress-driven nonlocal elasticity. In H. Altenbach, N. Chinchaladze, R. Kienzler, & W. Müller (Eds.), *Analysis of shells, plates, and beams. advanced structured materials*. Cham: Springer. vol 134.

Malikan, M., & Eremeyev, V. A. (2020b). On the geometrically nonlinear vibration of a piezo-flexomagnetic nanotube. *Mathematical Methods in the Applied Sciences*. https://doi.org/10.1002/mma.6758

Malikan, M., & Eremeyev, V. A. (2020c). On nonlinear bending study of a piezo-flexomagnetic nanobeam based on an analytical-numerical solution. *Nanomaterials, 10*, 1762. Article.

Malikan, M., & Eremeyev, V. A. (2021a). Flexomagneticity in buckled shear deformable hard-magnetic soft structures. *Continuum Mechanics and Thermodynamics, 34*, 1–16.

Malikan, M., & Eremeyev, V. A. (2021b). Flexomagnetic response of buckled piezomagnetic composite nanoplates. *Composite Structures, 267*, Article 113932. Article.

Malikan, M., & Eremeyev, V. A. (2021c). Effect of surface on the flexomagnetic response of ferroic composite nanostructures; nonlinear bending analysis. *Composite Structures, 271*, Article 114179. Article.

Malikan, M., Eremeyev, V. A., Chakraverty, S., Tornabene, F., & Reddy, J. N (2021d). On forced vibrations of piezo-flexomagnetic nano-actuator beams. *Modeling and computation in vibration problems. numerical and semi-Analytical methods*. IOP. vol 1.

Malikan, M., & Eremeyev, V. A. (2022a). The effect of shear deformations' rotary inertia on the vibrating response of multi-physic composite beam-like actuators. *Composite Structures, 297*, Article 115951. Article.

Malikan, M., & Eremeyev, V. A. (2022b). On a flexomagnetic behavior of composite structures. *International Journal of Engineering Science, 175*, Article 103671. Article.

Malikan, M., & Eremeyev, V. A. (2023a). On dynamic modeling of piezomagnetic/flexomagnetic microstructures based on Lord-Shulman thermoelastic model. *Archive of Applied Mechanics, 93*, 181–196.

Malikan, M., & Eremeyev, V. A. (2023b). On time-dependent nonlinear dynamic response of micro-elastic solids. *International Journal of Engineering Science, 182*, Article 103793. Article.

Malikan, M., Eremeyev, V. A., & Żur, K. K. (2020a). Effect of axial porosities on flexomagnetic response of in-plane compressed piezomagnetic nanobeams. *Symmetry, 12*, 1935. Article.

Malikan, M., Krasheninnikov, M., & Eremeyev, V. A. (2020c). Torsional stability capacity of a nano-composite shell based on a nonlocal strain gradient shell model under a three-dimensional magnetic field. *International Journal of Engineering Science, 148*, Article 103210. Article.

Malikan, M., & Nguyen, V. B. (2018). Buckling analysis of piezo-magnetoelectric nanoplates in hygrothermal environment based on a novel one variable plate theory combining with higher-order nonlocal strain gradient theory. *Physica E: Low-dimensional Systems and Nanostructures, 102*, 8–28.

Malikan, M., Tornabene, F., & Dimitri, R. (2018). Nonlocal three-dimensional theory of elasticity for buckling behavior of functionally graded porous nanoplates using volume integrals. *Materials Research Express, 5*, Article 095006. Article.

Malikan, M., Uglov, N. S., & Eremeyev, V. A. (2020b). On instabilities and post-buckling of piezomagnetic and flexomagnetic nanostructures. *International Journal of Engineering Science, 157*, 10339. Article.

Malikan, M., Wiczenbach, T., & Eremeyev, V. A. (2021). On thermal stability of piezo-flexomagnetic microbeams considering different temperature distributions. *Continuum Mechanics and Thermodynamics, 33*, 1281–1297.

Malikan, M., Wiczenbach, T., & Eremeyev, V. A. (2022a). Thermal buckling of functionally graded piezomagnetic micro and nanobeams presenting the flexomagnetic effect. *Continuum Mechanics and Thermodynamics, 34*, 1051–1066.

Malikan, M., Wiczenbach, T., & Eremeyev, V. A. (2022b). Flexomagneticity in functionally graded nanostructures. In H. Altenbach, V. A. Eremeyev, A. Galybin, & A. Vasiliev (Eds.), *Advanced materials modelling for mechanical, medical and biological applications. advanced structured materials*. Cham: Springer. vol 155.

Mallek-Zouari, I., Ben Taazayet, W., Grenèche, J. M., Bessais, L., Dkhil, B., & Thabet Mliki, N. (2023). Field-induced spin cycloidal modulation to antiferromagnetic transition and possible flexomagnetic effect in BiFeO3 nanoparticles. *Journal of Alloys and Compounds, 934*, Article 167944. Article.

Markov, M., Markov, A., Levin, V., & Sabina, F. J. (2022). Electromagnetic field generated by acoustic wave scattering at a poroelastic inclusion located in a fluid. *International Journal of Engineering Science, 181*, Article 103766. Article.

Mohamed, A. S. Y. (2017). Smart Materials Innovative Technologies in architecture; Towards Innovative design paradigm. *Energy Procedia, 115*, 139–154.

Naskar, S., Shingare, K. B., Mondal, S., & Mukhopadhyay, T. (2022). Flexoelectricity and surface effects on coupled electromechanical responses of graphene reinforced functionally graded nanocomposites: A unified size-dependent semi-analytical framework. *Mechanical Systems and Signal Processing, 169*, Article 108757. Article.

Poplawski, B., Mikułowski, G., Orłowska, A., & Jankowski, L. (2021). On/off nodal reconfiguration for global structural control of smart 2D frames. *Journal of Applied and Computational Mechanics, 7*(Special Issue), 1121–1129.

Qu, Y., Jin, F., & Yang, J. (2021). Torsion of a flexoelectric semiconductor rod with a rectangular cross section. *Archive of Applied Mechanics, 91*, 2027–2038.

Russillo, A. F., Failla, G., Barretta, R., & Marotti de Sciarra, F. (2022). On the dynamics of 3D nonlocal solids. *International Journal of Engineering Science, 180*, Article 103742. Article.

Sabirianov, R. F., & Lukashev, P (2010). Magneto-elastic properties of frustrated triangular magnetic structure: Flexomagnetic effect. *American Physical Society*. APS March Meeting 2010, abstract id. Q34.008.

Shahmohammadi, M. A., Mirfatah, S. M., Salehipour, H., & Civalek, Ö. (2023). On nonlinear forced vibration of micro scaled panels. *International Journal of Engineering Science, 182*, Article 103774. Article.

Shao Ong, O. Z., Ghayesh, M. H., & Losic, D. (2023). Vibrations of porous functionally graded CNT reinforced viscoelastic beams connected via a viscoelastic layer. *International Journal of Engineering Science, 191*, Article 103917. Article.

Sahmani, S., & Safaei, B. (2022). Nonlinear three-dimensional oscillations of probabilistic reinforced nanocomposite shells at microscale via modified strain gradient meshfree formulations. *Proceedings of the Institution of Mechanical Engineers, Part C: Journal of Mechanical Engineering Science, 237*. https://doi.org/10.1177/09544062221142144

Shu, L., Wei, X., Pang, T., Yao, X., & Wang, C. (2011). Symmetry of flexoelectric coefficients in crystalline medium. *Journal of Applied Physics, 110*, Article 104106. Article.

Sladek, J., Sladek, V., Xu, M., & Deng, Q. (2021). A cantilever beam analysis with flexomagnetic effect. *Meccanica, 56*, 2281–2292.

Sidhardh, S., & Ray, M. C. (2018). Flexomagnetic response of nanostructures. *Journal of Applied Physics, 124*, Article 244101. Article.

Singh, D., Kiran, R., Chawla, K., Kumar, R., Chauhan, V. S., & Vaish, R. (2022). Determination of multi-physics effective properties, and actuation response of triply periodic minimal surface based novel photostrictive composites: A finite element analysis. *International Journal of Engineering Science, 178*, Article 103726. Article.

23

Singhal, A., Sedighi, H. M., Ebrahimi, F., & Kuznetsova, I. (2021). Comparative study of the flexoelectricity effect with a highly/weakly interface in distinct piezoelectric materials (PZT-2, PZT-4, PZT-5H, LiNbO₃, BaTiO₃). *Waves in Random and Complex Media, 31*, 1780–1798.

Stempin, P., & Sumelka, W. (2022). Space-fractional small-strain plasticity model for microbeams including grain size effect. *International Journal of Engineering Science, 175*, Article 103672. Article.

Stempin, P., Pawlak, T. P., & Sumelka, W. (2023). Formulation of non-local space-fractional plate model and validation for composite micro-plates. *International Journal of Engineering Science, 192*, Article 103932. Article.

Torabi, J., Niiranen, J., & Ansari, R. (2021). Nonlinear finite element analysis within strain gradient elasticity: Reissner-Mindlin plate theory versus three-dimensional theory. *European Journal of Mechanics - A/Solids, 87*, Article 104221. Article.

Ud Din, I., Aslam, N., Medhin, Y., Sikandar Bathusha, M. S., Irfan, M. S., Umer, R., & Khan, K. A. (2022). Electromechanical behavior of self-sensing composite sandwich structures for next generation more electric aerostructures. *Composite Structures, 300*, Article 116169. Article.

Vijay, K., Varadan, K., Vinoy, J., & Gopalakrishnan, S. (2006). *Smart material systems and mems: Design and development methodologies*. John Wiley & Sons, Ltd. https://onlinelibrary.wiley.com/doi/book/10.1002/0470093633.

Wittrick, W. H. (1987). Analytical, three-dimensional elasticity solutions to some plate problems, and some observations on Mindlin's plate theory. *International Journal of Solids and Structures, 23*, 441–464.

Xu, X., Karami, B., & Janghorban, M. (2021c). On the dynamics of nanoshells. *International Journal of Engineering Science, 158*, Article 103431. Article.

Xu, X., Karami, B., & Shahsavari, D. (2021a). Time-dependent behavior of porous curved nanobeam. *International Journal of Engineering Science, 160*, Article 103455. Article.

Xu, X., Shahsavari, D., & Karami, B. (2021b). On the forced mechanics of doubly-curved nanoshell. *International Journal of Engineering Science, 168*, Article 103538. Article.

Yee, K., & Ghayesh, M. H. (2023). A review on the mechanics of graphene nanoplatelets reinforced structures. *International Journal of Engineering Science, 186*, Article 103831. Article.

Yurkov, A. S., & Yudin, P. V. (2023). Continuum model for converse flexoelectricity in a thin plate. *International Journal of Engineering Science, 182*, Article 103771.

Zafarmand, H., & Kadkhodayan, M. (2015). Three dimensional elasticity solution for static and dynamic analysis of multi-directional functionally graded thick sector plates with general boundary conditions. *Composites Part B: Engineering, 69*, 592–602.

Zhang, G. Y., Guo, Z. W., Qu, Y. L., Gao, X. L., & Jin, F. (2022b). A new model for thermal buckling of an anisotropic elastic composite beam incorporating piezoelectric, flexoelectric and semiconducting effects. *Acta Mechanica, 233*, 1719–1738.

Zhang, N., Zheng, S., & Chen, D. (2022a). Size-dependent static bending, free vibration and buckling analysis of curved flexomagnetic nanobeams. *Meccanica, 57*, 1505–1518.

Zhang, N., Zheng, Sh., & Chen, D. (2019). Size-dependent static bending of flexomagnetic nanobeams. *Journal of Applied Physics, 126*, Article 223901. Article.

Zhang, Y. W., She, G. L., & Ding, H. X. (2023). Nonlinear resonance of graphene platelets reinforced metal foams plates under axial motion with geometric imperfections. *European Journal of Mechanics - A/Solids, 98*, Article 104887. Article.

Zheng, Y., Karami, B., & Shahsavari, D. (2022). On the vibration dynamics of heterogeneous panels under arbitrary boundary conditions. *International Journal of Engineering Science, 178*, Article 103727. Article.

Zhou, Sh., Li, A., & Wang, B. (2016). A reformulation of constitutive relations in the strain gradient elasticity theory for isotropic materials. *International Journal of Solids and Structures, 80*, 28–37.